

# Higher-dimensional soliton generation, stability and excitations of the $\mathcal{PT}$ -symmetric nonlinear Schrödinger equations

Yong Chen<sup>1</sup>, Zhenya Yan<sup>2,3,\*</sup>, Boris A. Malomed<sup>4,5</sup>

<sup>1</sup> School of Mathematics and Statistics, Jiangsu Normal University, Xuzhou 221116, China

<sup>2</sup> Key Lab of Mathematics Mechanization, Academy of Mathematics and Systems Science, Chinese Academy of Sciences, Beijing 100190, China

<sup>3</sup> School of Mathematical Sciences, University of Chinese Academy of Sciences, Beijing 100049, China

<sup>4</sup> Department of Physical Electronics, School of Electrical Engineering, Faculty of Engineering, and Center for Light-Matter Interaction, Tel Aviv University, Tel Aviv 69978, Israel

<sup>5</sup> Instituto de Alta Investigación, Universidad de Tarapacá, Casilla 7D, Arica, Chile

**Abstract.** We study a class of physically intriguing  $\mathcal{PT}$ -symmetric generalized Scarf-II (GS-II) potentials, which can support exact solitons in one- and multi-dimensional nonlinear Schrödinger equation. In the 1D and multi-D settings, we find that a properly adjusted localization parameter may support fully real energy spectra. Also, continuous families of fundamental and higher-order solitons are produced. The fundamental states are shown to be stable, while the higher-order ones, including 1D multimodal solitons, 2D solitons, and 3D light bullets, are unstable. Further, we find that the stable solitons can always propagate, in a robust form, remaining trapped in slowly moving potential wells of the GS-II type, which opens the way for manipulations of optical solitons. Solitons may also be transformed into stable forms by means of adiabatic variation of potential parameters. Finally, an alternative type of  $n$ -dimensional  $\mathcal{PT}$ -symmetric GS-II potentials is reported too. These results will be useful to further explore the higher-dimensional  $\mathcal{PT}$ -symmetric solitons and to design the relative physical experiments.

*Keywords:* Higher-dimensional nonlinear Schrödinger equation;  $\mathcal{PT}$ -symmetric potentials; stable solitons; adiabatic management

## 1 Introduction

In the classical quantum mechanics (QM), a Hamiltonian is usually required to be hermitian, as the resulting spectra predict physically relevant real eigenvalues of energy. However, the hermiticity of the Hamiltonian is not a necessary condition to secure its real spectra. In this respect, the concept of non-Hermitian  $\mathcal{PT}$ -symmetric Hamiltonian, first put forward by Bender and Boettcher in 1998 [1], is a noteworthy generalization of classical QM, where  $\mathcal{P}$  and  $\mathcal{T}$  are defined as  $\mathcal{P} : x \rightarrow -x$  and  $\mathcal{T} : i \rightarrow -i$ . Such Hamiltonian include the complex potentials whose real and imaginary parts are spatially even and odd, respectively. The  $\mathcal{PT}$ -symmetric Hamiltonians exhibit fully real spectra, provided that the strength of the imaginary part of the potential does not exceed a critical value [1–6]. The natural nonlinear extension of  $\mathcal{PT}$ -symmetric models produce diverse stable localized modes ( $\mathcal{PT}$ -symmetric solitons) [7, 8, 10–15, 43]. Fundamentally fascinating features associated with the  $\mathcal{PT}$  symmetry, including symmetry breaking and presence of exceptional points in the spectrum, have been investigated theoretically and observed experimentally in many physical systems [16–26].

In particular, the  $\mathcal{PT}$  symmetry can be realized in optics by introducing mutually symmetric gain and loss elements in the waveguide geometry, which are represented by the above-mentioned spatially odd imaginary part of the effective potential [7, 27]. In other words, the respective complex refractive-index distribution may play the role of  $\mathcal{PT}$ -symmetric optical potentials. Particularly, in periodic photonic-lattice potentials, a large number of new phenomena, maintained by the  $\mathcal{PT}$ -symmetry, have been discovered, such as the double refraction, power oscillations, phase singularities, and secondary emission [28–30].

---

\*Email address: zyyan@mmrc.iss.ac.cn (Corresponding author)

In the last decade, increasing attention has been drawn to exploring one- and high-dimensional solitons in nonlinear media with specially designed effective potentials, including the well-known ones of the Scarf-II type [7, 11, 13, 31, 32], Gaussian [10, 33, 34], harmonic oscillator [32, 35], Rosen-Morse [36], double-delta [37, 38], super-Gaussian [39], optical lattices and superlattices [12, 40–44], time-dependent harmonic-Gaussian potential [15], anharmonic sextic double well [14], and others. Various effective potentials have been developed in photonics [45] and other physical media [46–56]. Families of non-parity-time-symmetric solitons are also admitted in parity-time-symmetric potentials [57].

Recently, a broad variety of  $\mathcal{PT}$ -symmetric nonlinear localized modes and their stability were addressed in the framework of generalized nonlinear Schrödinger (NLS) equations with variable group-velocity coefficients [58, 59], third-order dispersion [60] and position-dependent effective mass [61], as well as derivative [62], nonlocal [63], and other generalized nonlinearities [64], and in the three-wave-interaction model [65]. Localized states in a nearly- $\mathcal{PT}$ -symmetric Ginzburg-Landau model were considered too [66]. Stable solitons of peakon and flat-top types can be maintained by  $\mathcal{PT}$ -symmetric potentials combining terms with  $\delta(x)$  and  $|x|$  [67]. Also, stable solitons pinned to attraction centers combined with parity-time-symmetric  $\delta$ -functional dipoles in the 1D system with the critical and supercritical self-focusing nonlinearity were reported [68, 69]. Stable solitons in the 2D  $\mathcal{PT}$ -symmetric potentials were found in [70] and examples of stable asymmetric solitons in 3D settings were provided in [71]. More vortex solitons in various physical contexts were reviewed in Ref. [72]. Theoretical and experimental findings for diverse nonlinear modes in  $\mathcal{PT}$ -symmetric media are summarized in several recent reviews [45, 73–79].

Nonlinear modes supported by  $\mathcal{PT}$ -symmetric potentials remain a relevant topic for ongoing studies [73]. In this paper, we develop an analytical treatment and numerical investigation of nonlinear localized modes, represented in an integral-convolution form, in one-, two-, and three-dimensional (1D, 2D, and 3D) NLS equations with a novel category of  $\mathcal{PT}$ -symmetric generalized Scarf-II potentials.

The rest of this paper is organized as follows. First, the linear spectral problem with the  $\mathcal{PT}$ -symmetric potential is considered in Sec. 2. Next, Sec. 3 addresses 1D, 2D and 3D nonlinear localized modes and their dynamical characteristics, such as stability and excitation in  $\mathcal{PT}$ -symmetric GS-II double-well potentials in the presence of the Kerr nonlinearity. Importantly, the corresponding  $n$ -dimensional solitons are obtained in an exact form. In Sec. 4, another type of  $\mathcal{PT}$ -symmetric GS-II potentials are produced, and the corresponding 3D nonlinear localized modes are investigated, including their stability. The paper is concluded by Sec. 5.

## 2. The higher-dimensional $\mathcal{PT}$ -symmetric NLS equation

In Kerr-nonlinear optical media with complex-valued external potentials, the transmission of optical beams is governed by the following generalized NLS equation written in the dimensionless form [7, 8]:

$$i\frac{\partial\psi}{\partial z} + [\nabla_x^2 + V(x) + iW(x) + g|\psi|^2]\psi = 0, \quad (1)$$

where the complex envelope field  $\psi \equiv \psi(x, z) \in \mathbb{C}[x, z]$  is the slowly-varying light-field amplitude,  $x = (x_1, \dots, x_n)$  are coordinates in the  $n$ -dimensional space, *viz.*,  $x = x$  and  $(x, y)$  in the 1D and 2D waveguides, whereas in the 3D space, the additional coordinate is the temporal one,  $x = (x, y, t)$ ,  $\nabla_x$  is the  $n$ -dimensional gradient operator,  $\nabla_x^2 = \sum_{j=1}^n \partial_{x_j}^2$  is the Laplacian operator,  $z$  is the propagation distance, and  $g$  defines the self-focusing ( $g = 1$ ) or defocusing ( $g = -1$ ) sign of the cubic nonlinearity. The complex potential  $V(x) + iW(x)$  is  $\mathcal{PT}$ -symmetric under the constraints  $V(x) = V(-x)$ ,  $W(-x) = -W(x)$ . In the optical waveguide, the real part  $V(x)$  of the potential is proportional to local value of refractive index, while the imaginary part  $W(x)$  represents the gain (amplification) or loss (absorption) in the medium.

Under the present assumptions, Eq. (1) is invariant under the combined actions of the parity- and time-reflection, defined as  $\mathcal{P} : x \rightarrow -x$ ;  $\mathcal{T} : i \rightarrow -i, z \rightarrow -z$ , respectively. The invariance implies that if  $\psi(x, z)$  is an exact solution of Eq. (1), so is  $\mathcal{PT}\psi(x, z) = \psi^*(-x, -z)$ . Usually, analytically available solutions of Eq. (1) are  $\mathcal{PT}$ -symmetric,

i.e., they are converted into themselves by the  $\mathcal{PT}$  transform. Eq. (1) can also be written in the variational form,  $i\psi_z = \delta\mathcal{H}(\psi)/(\delta\psi^*)$ , with the generalized Hamiltonian

$$\mathcal{H} = \int_{\mathbb{R}^n} \left\{ |\nabla_x \psi|^2 - [V(\mathbf{x}) + iW(\mathbf{x})] |\psi|^2 - \frac{g}{2} |\psi|^4 \right\} d\mathbf{x}, \quad (2)$$

where the asterisk stands for the complex conjugate. Because the Hamiltonian is not real, Eq. (1) does not conserve the total power,  $P(z) = \int_{\mathbb{R}^n} |\psi(\mathbf{x}, z)|^2 d\mathbf{x}$ . The evolution equation for the power follows from Eq. (1):

$$\frac{dP(z)}{dz} = -2 \int_{\mathbb{R}^n} W(\mathbf{x}) |\psi(\mathbf{x}, z)|^2 d\mathbf{x}. \quad (3)$$

In particular, if the local intensity,  $|\psi(\mathbf{x}, z)|^2$ , is an even function of  $\mathbf{x}$ , as is usually the case for stationary modes, while the  $\mathcal{PT}$  symmetry demands  $W(\mathbf{x})$  to be an odd function of  $\mathbf{x}$ , Eq. (3) yields  $dP/dz = 0$ , that is, the total power is conserved for such solutions.

## 2.1 The analysis of nonlinear modes

In general, Eq. (1) with complex potential  $V(\mathbf{x}) + iW(\mathbf{x})$  is a non-integrable equation, as the Lax pair, which is necessary for the integrability, is available only in rare special cases [11]. In the absence of the integrability, classical methods for constructing exact solutions, such as the bilinear Hirota technique and Darboux transformation, cannot be used. Therefore, we here aim to find nonlinear modes as steady-state solutions,  $\psi(\mathbf{x}, z) = \phi(\mathbf{x}) e^{i\mu z}$  with a real propagation constant  $\mu$ . The wave function  $\phi(\mathbf{x})$ , which is assumed to vanish at  $|\mathbf{x}| \rightarrow \infty$ , as we look for localized states, satisfies the stationary version of Eq. (1):

$$\left( \nabla_x^2 - \mu \right) \phi = - \left[ V(\mathbf{x}) + iW(\mathbf{x}) + g|\phi|^2 \right] \phi. \quad (4)$$

This complex-valued wave function  $\phi(\mathbf{x})$  can be further expressed in the Madelung form

$$\phi(\mathbf{x}) = u(\mathbf{x}) e^{i\varphi(\mathbf{x})}, \quad (5)$$

with real  $u(\mathbf{x})$  and  $\varphi(\mathbf{x})$  being, respectively, real amplitude and phase. The substitution of the Madelung ansatz into Eq. (4) leads to coupled nonlinear equations

$$\begin{aligned} \nabla_x \cdot \left( u^2(\mathbf{x}) \nabla_x \varphi(\mathbf{x}) \right) &= -W(\mathbf{x}) u^2(\mathbf{x}), \\ \Delta_x u(\mathbf{x}) &= [-V(\mathbf{x}) - g u^2(\mathbf{x}) + \nabla_x \varphi(\mathbf{x}) \cdot \nabla_x \varphi(\mathbf{x}) + \mu] u(\mathbf{x}). \end{aligned} \quad (6)$$

In particular, for the 1D case:  $\mathbf{x} \rightarrow x$ , let  $\varphi(x) = \int_0^x v(s) ds$ , that is,

$$\phi(x) = u(x) \exp \left[ i \int_0^x v(s) ds \right],$$

with real  $u(x)$  and  $v(x)$  being, respectively, real amplitude and hydrodynamic velocity. Then system (6) becomes

$$\begin{aligned} v(x) &= -u^{-2}(x) \int_0^x W(s) u^2(s) ds, \\ \partial_x^2 u(x) &= [-V(x) - g u^2(x) + v^2(x) + \mu] u(x). \end{aligned}$$

## 2.2 Representation of general solutions

To seek soliton solutions of Eq. (4), we restrict them to the *Schwartz space* of rapidly-decreasing functions [80]

$$\phi(\mathbf{x}) \in \wp(\mathbb{R}^n) = \{f(\mathbf{x}) \in C^\infty(\mathbb{R}^n) \mid \lim_{|\mathbf{x}| \rightarrow \infty} \mathbf{x}^\alpha \partial^p f(\mathbf{x}) = 0, \forall \alpha, p \in \mathbb{N}^n\},$$

where  $x^\alpha \partial^p f(x) \equiv x_1^{\alpha_1} \cdots x_n^{\alpha_n} \partial_{x_1}^{p_1} \cdots \partial_{x_n}^{p_n} f(x)$  and  $C^\infty(\mathbb{R}^n)$  represents the space consisting of infinitely continuous differentiable complex-valued functions.

We assume that the trapping potential selects solutions with  $\mu > 0$ . The Green-function equation corresponding to Eq. (4) is

$$\nabla_{\mathbf{x}}^2 G - \mu G = \delta(\mathbf{x}) = \delta(x_1)\delta(x_2) \cdots \delta(x_n). \quad (7)$$

Applying the Fourier transform to Eq. (7) and then the inverse transform leads to the expression for the Green's function (fundamental solution),

$$G(\mathbf{x}) = -\frac{1}{(2\pi)^n} \int_{\mathbb{R}^n} \frac{e^{i\mathbf{x}\cdot\boldsymbol{\xi}}}{|\boldsymbol{\xi}|^2 + \mu} d\boldsymbol{\xi}. \quad (8)$$

Then, solutions of Eq. (4) can be represented in the form of the convolution with the Green's function:

$$\phi_G(\mathbf{x}) = -G(\mathbf{x}) * [V(\mathbf{x})\phi + iW(\mathbf{x})\phi + g|\phi|^2\phi]. \quad (9)$$

Further, Eq. (9) can be written in a more specific form:

$$\tilde{\phi} = C_1 \exp\left(\sum_{k=1}^n \beta_k x_k\right) + C_2 \exp\left(\sum_{k=1}^{n-1} \beta_k x_k - \beta_n x_n\right) - \int_{\mathbb{R}^n} G(\mathbf{x} - \mathbf{y}) [V(\mathbf{y}) + iW(\mathbf{y}) + g|\phi(\mathbf{y})|^2] \phi(\mathbf{y}) d\mathbf{y}. \quad (10)$$

where  $\beta_n = \sqrt{\mu - \sum_{k=1}^{n-1} \beta_k^2}$ , and  $C_1, C_2, \beta_k (k = 1, 2, \dots, n-1)$  are arbitrary complex constants. In particular,

- In the 1D setting, Eq. (10) reduces to

$$\tilde{\phi}(x) = C_1 e^{\sqrt{\mu}x} + C_2 e^{-\sqrt{\mu}x} - \int_{\mathbb{R}^n} G(x - x') [V(x') + iW(x') + g|\phi(x')|^2] \phi(x') dx'. \quad (11)$$

- In the 2D case, Eq. (10) becomes

$$\begin{aligned} \tilde{\phi}(x, y) = & C_1 e^{\beta x + \sqrt{\mu - \beta^2} y} + C_2 e^{\beta x - \sqrt{\mu - \beta^2} y} - \int_{\mathbb{R}^2} G(x - x', y - y') [V(x', y') + iW(x', y') \\ & + g|\phi(x', y')|^2] \phi(x', y') dx' dy', \end{aligned} \quad (12)$$

where  $\beta$  is an arbitrary real constant.

### 2.3 The iteration scheme for constructing numerical nonlinear modes

Define the Fourier transform  $\mathcal{F}$  of  $\phi(\mathbf{x})$  by

$$\hat{\phi}(\boldsymbol{\xi}) = \mathcal{F}[\phi(\mathbf{x})] = \frac{1}{(\sqrt{2\pi})^n} \int_{\mathbb{R}^n} \phi(\mathbf{x}) e^{-i\mathbf{x}\cdot\boldsymbol{\xi}} d\boldsymbol{\xi}.$$

Applying this transform to Eq. (4) yields

$$\hat{\phi}(\boldsymbol{\xi}) = \frac{\mathcal{F}[V(\mathbf{x})\phi] + i\mathcal{F}[W(\mathbf{x})\phi] + g\mathcal{F}[|\phi|^2\phi]}{|\boldsymbol{\xi}|^2 + \mu}. \quad (13)$$

To secure the convergence of the iterative scheme, a new field variable is usually introduced,  $\phi(\mathbf{x}) = \gamma\Phi(\mathbf{x})$ , where  $\gamma$  is a nonzero constant to be determined, hence  $\hat{\phi}(\boldsymbol{\xi}) = \gamma\hat{\Phi}(\boldsymbol{\xi})$ . Then Eq. (13) becomes

$$\hat{\Phi}(\boldsymbol{\xi}) = \frac{\mathcal{F}[V\Phi] + i\mathcal{F}[W\Phi] + g\mathcal{F}[|\gamma|^2|\Phi|^2\Phi]}{|\boldsymbol{\xi}|^2 + \mu} \triangleq G_\gamma(\boldsymbol{\xi}).$$

Multiplying it by  $\hat{\Phi}^*(\xi)$  and integrating over the entire  $\xi$  space leads to an equation for  $\gamma$ ,

$$\int_{\mathbb{R}^n} \left( |\hat{\Phi}(\xi)|^2 - \hat{\Phi}^*(\xi) G_\gamma(\xi) \right) d\xi = 0. \quad (14)$$

Thus, the iteration scheme of for constructing numerical nonlinear modes is defined as

$$\hat{\Phi}_{m+1} = \frac{\mathcal{F}[V\Phi_m] + i\mathcal{F}[W\Phi_m] + g\mathcal{F}[|\gamma_m|^2|\Phi_m|^2\Phi_m]}{|\xi|^2 + \mu}, \quad (15)$$

where  $\gamma_m$  is determined by Eq. (14) with  $\Phi = \Phi_m$ ,  $\gamma = \gamma_m$ .

Other numerical algorithms can also be employed to solve Eq. (4) with the zero boundary conditions, such as the classical shooting method for 1D fundamental and higher-order solitons, spectral renormalization method for multidimensional self-localized states [81], the modified squared-operator iteration method [82], as well as the Newton's conjugate-gradient method for multidimensional and higher-order nonlinear modes [83]. We here make use of the modified squared-operator iteration method to search for higher-order numerical nonlinear modes, as it allows us to reach higher precision, and is convenient for the application in higher dimensions. Besides, the combination of the Fourier pseudospectral method and split-step algorithm are used to simulate the propagation of nonlinear modes [84].

While most results in this area are obtained in the fully numerical form, for particular types of  $\mathcal{PT}$  potential wells, exact nonlinear modes play a crucial role in seeking families of stable numerical solitons (see, e.g., Refs. [13–15]).

## 2.4 The stability analysis of nonlinear modes

When nonlinear localized modes of Eq. (1) are obtained in the form of expression  $\psi(x, z) = \phi(x)e^{i\mu z}$ , exact or numerical, one can analyze their linear stability by perturbing them as follows:

$$\psi(x, z) = \left[ \phi(x) + \varepsilon \left( f_1(x)e^{i\nu z} + f_2^*(x)e^{-i\nu^* z} \right) \right] e^{i\mu z}, \quad (16)$$

where  $|\varepsilon| \ll 1$  is an amplitude of the small perturbation, both  $f_1(x)$  and  $f_2(x)$  are perturbation eigenfunctions, and  $\nu$  is the (in)stability eigenvalue. Substituting the perturbed solutions in Eq. (1) and linearizing it with respect of  $\varepsilon$ , gives rise to the following linear-stability eigenvalue problem

$$\begin{pmatrix} \tilde{L} - \nu & g\phi^2(x) \\ -g\phi^{*2}(x) & -\tilde{L}^* - \nu \end{pmatrix} \begin{pmatrix} f_1(x) \\ f_2(x) \end{pmatrix} = 0 \quad (17)$$

with  $\tilde{L} = \nabla_x^2 + [V(x) + iW(x)] + 2g|\phi(x)|^2 - \mu$ .

The steady-state nonlinear modes  $\phi(x)e^{i\mu z}$  are linearly unstable once  $\nu$  has a negative imaginary part, otherwise they are stable. The celebrated Fourier collocation method is a practical and efficient tool to compute the entire linear-stability spectrum [84]. While the linear-stability analysis roughly predicts a parameter range corresponding to stability of nonlinear modes, it provides only necessary but not sufficient condition for the true nonlinear stability. The full stability should be then tested by means of direct numerical simulations of the perturbed evolution.

## 2.5 $\mathcal{PT}$ -symmetry breaking in the GS-II potential

In this subsection, we concentrate on the  $\mathcal{PT}$ -symmetric breaking phenomena in the linear regime, based on the equation

$$\mathcal{L}\Psi(x) = \lambda\Psi(x), \quad \mathcal{L} = -\frac{d^2}{dx^2} - V(x) - iW(x), \quad (18)$$

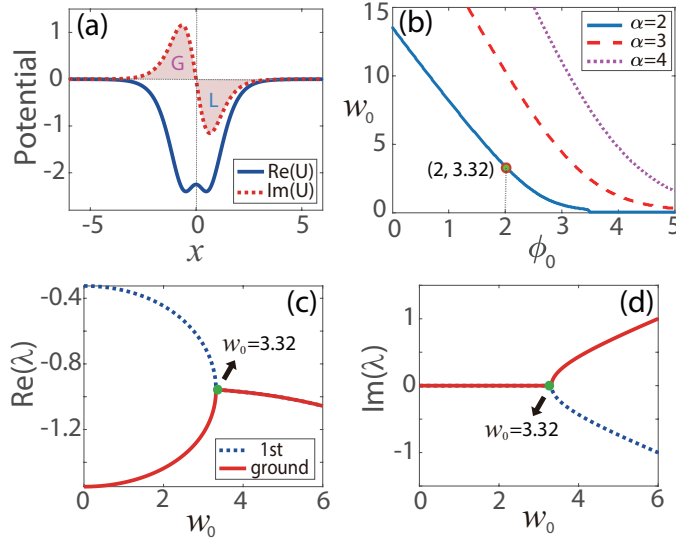


Figure 1: (color online). (a) The profile of 1D  $\mathcal{PT}$ -symmetric GS-II potential  $U = -V(x) - iW(x)$ , defined by Eqs. (19) and (20) with  $\alpha = 2, \phi_0 = 2, w_0 = 3$ , and  $g = 1$ , where 'G' ('L') denotes the gain (loss) region. (b) Boundaries of the  $\mathcal{PT}$ -symmetry breaking in the  $(\phi_0, w_0)$  plane of the linear system (18) [with no cubic term in Eq. (1)] for  $\alpha = 2, 3, 4$ . The  $\mathcal{PT}$  symmetry is unbroken under the boundaries. (c) Real and (d) imaginary parts of eigenvalues  $\lambda$  of the two lowest states as a function of  $w_0$ , for  $\alpha = 2, \phi_0 = 2$ .

with the 1D  $\mathcal{PT}$ -symmetric GS-II potential taken as

$$V(x) = v_1 \text{sech}^2 x + v_2 \text{sech}^{2\alpha} x, \quad W(x) = w_0 \text{sech}^\alpha x \tanh x, \quad (19)$$

where  $\alpha > 0$  (the *localization parameter*),  $v_1 > 0, v_2$ , and  $w_0$  are real parameters, while  $\lambda$  and  $\Psi(x)$  represent the discrete spectrum and the corresponding bound-state eigenfunctions. This  $\mathcal{PT}$ -symmetric potential with  $\alpha = 1$  and  $v_1 > 0, v_2 = 0$  (or  $v_1 > -v_2 \neq 0$ ) reduces to the classical Scarf-II potential [7,85]. Another version of the GS-II potential, quite different from the one written in Eq. (19), was considered in Ref. [61].

To find exact nonlinear localized modes produced by Eq. (4), in what follows we focus on a special case of potential (19) with

$$v_1 = \alpha(\alpha + 1), \quad v_2 = w_0^2 / (9\alpha^2) - g\phi_0^2, \quad (20)$$

where  $\phi_0$  is a new real-valued parameter in place of  $v_2$ . In this case, coefficient  $w_0$  independently determines the strength of the gain-loss distribution  $W(x)$ . Once both  $\alpha$  and  $w_0$  are fixed, one can choose any value of  $v_2$  in Eq. (20) by means of adjusting coefficient  $\phi_0$ . Note that when the gain-loss strength  $w_0$  or potential index  $\alpha$  changes, both real and imaginary parts of the GS-II potential (19) alter, which may lead to several distinct  $\mathcal{PT}$ -symmetry-breaking scenarios.

Without loss of generality, we assume  $\phi_0 \geq 0, w_0 \geq 0$ , and  $g = 1$  (the latter condition implies that the Kerr nonlinearity is self-focusing), unless specified otherwise. For illustration, a representative  $\mathcal{PT}$ -symmetric double-well GS-II potential, as well as the corresponding gain and loss regions are exhibited in Fig. 1(a).

Next, we look for all-real spectra in  $\mathcal{PT}$ -symmetric GS-II potential (19) by solving the linear eigenvalue problem (18). Note that, with  $\alpha = 1$ , the GS-II potential (19) with coefficients (20) reduces to the same form as considered in Ref. [86], where the exact condition of the persistence of the unbroken  $\mathcal{PT}$ -symmetric phases was derived:

$$\phi_0 \leq \frac{|2w_0 - 9|}{6}. \quad (21)$$

At  $\alpha \neq 1$ , we have found the  $\mathcal{PT}$ -symmetry-breaking boundary by means of the numerical Fourier spectral method. The boundaries are displayed for  $\alpha = 2, 3, 4$  in the first quadrant of the  $(\phi_0, w_0)$  parameter plane in Fig. 1(b). It is seen that the boundaries have a monotonous shape, approaching to zero with the increase of  $\phi_0$ . This happens because, as  $\phi_0$  increases, hence  $v_2$  decreases in Eq. (20), then the real part  $-V_0(x)$  of the GS-II potential (19) gradually turns from a potential well into a barrier, thereby leading to the emergence of complex eigenvalues and dramatic shrinkage of existence region for fully-real spectra. On the other hand, it is also seen that, with the growth of  $\alpha$ , the  $\mathcal{PT}$ -symmetry-breaking boundary rises higher, helping to expand the region of the unbroken  $\mathcal{PT}$  symmetry. In fact, due to the growth of  $\alpha$ , the potential well  $V(x)$  gets deeper, while the gain-loss distribution  $W(x)$  becomes tighter, hence more likely resulting in real eigenvalues. Thus, a conclusion is that the range of the totally-real spectra that the GS-II potential (19) produces can be enlarged by increasing  $\alpha$ .

It follows from Fig. 1(b) that, for the fixed  $\phi_0 = 2$ , the  $\mathcal{PT}$  symmetry-breaking threshold point is  $w_0 = 3.32$ . To illustrate the picture in detail, the evolution of the eigenvalues of the two lowest eigenstates following the change of coefficient  $w_0$  in Eq. (20) is shown in Figs. 1(c,d), where the eigenvalues remain completely real at  $w < w_0 = 3.32$ , while at  $w > w_0$  they form a complex-conjugate pair, produced by the bifurcation that takes place at  $w = w_0$ . In fact, the formal solutions with complex eigenvalues represent the so-called ghost states (that do not exist as stationary ones, but may represent long-lived unsteady ones [87–89]).

Similar  $\mathcal{PT}$ -symmetry-breaking phenomenology occurs in the multi-dimensional linear system. However, the key problem is how to generalize the GS-II potential (19) to the  $n$ -dimensional case, so as to be able to find exact nonlinear localized modes. As an example, we give the corresponding 2D GS-II potential:

$$\begin{aligned} V(x, y) &= \sum_{x_j} (v_1 \operatorname{sech}^2 x_j + v_{21} \operatorname{sech}^{2\alpha} x_j) + v_{22} \prod_{x_j} \operatorname{sech}^{2\alpha} x_j, \\ W(x, y) &= w_0 \sum_{x_j} \operatorname{sech}^\alpha x_j \tanh x_j, \end{aligned} \quad (22)$$

where  $x_j = x, y$ , and  $v_1, v_{21}$  and  $v_{22}$  are real constants with the 2D counterpart of Eq. (20) being

$$v_1 = \alpha(\alpha + 1), \quad v_{21} = w_0^2 / (9\alpha^2), \quad v_{22} = -g\phi_0^2. \quad (23)$$

$\mathcal{PT}$ -symmetry-breaking boundaries in this 2D system can be identified in the numerical form, similar to how it is shown above for 1D.

Lastly, the 3D GS-II potential can be obtained too, in the following form:

$$\begin{aligned} V(x, y, t) &= \sum_{x_j} (v_1 \operatorname{sech}^2 x_j + v_{21} \operatorname{sech}^{2\alpha} x_j) + v_{22} \prod_{x_j} \operatorname{sech}^{2\alpha} x_j, \\ W(x, y, t) &= w_0 \sum_{x_j} \operatorname{sech}^\alpha x_j \tanh x_j, \end{aligned} \quad (24)$$

where  $x_j = x, y, t$ , and  $v_1, v_{21}, v_{22}, w_0$  are determined by Eq. (23).

### 3 Nonlinear modes and stability in the $\mathcal{PT}$ -symmetric GS-II potential

In this section, we firstly produce particular solutions for 1D, 2D and 3D exact nonlinear localized modes in the nonlinear system (1) with the GS-II potential (19). Then we numerically explore families of fundamental solitons including such exact modes, and the corresponding high-order nonlinear modes. The dynamical stability of these states is investigated in detail. In the end, we summarize the results obtained for the nonlinear localized states in the  $n$ -dimensional  $\mathcal{PT}$ -symmetric GS-II potential.

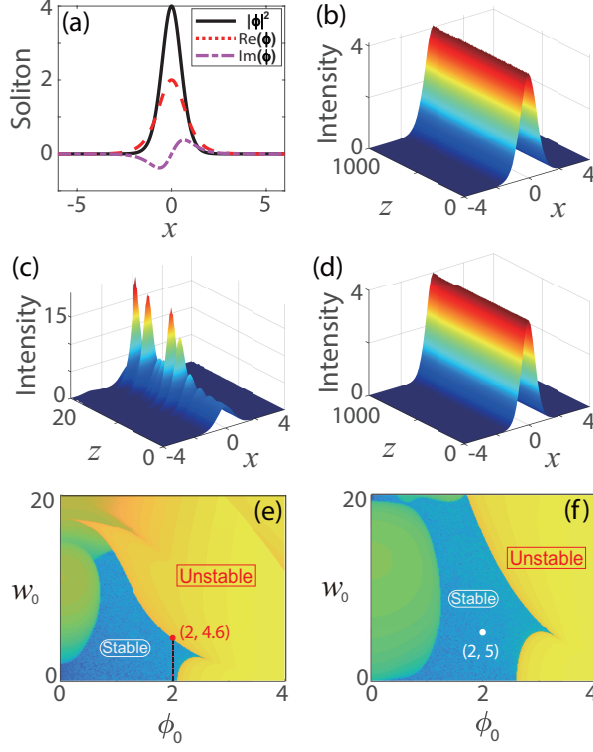


Figure 2: (a) The 1D exact fundamental soliton with  $\alpha = 2, \phi_0 = 2, w_0 = 3$ , and (b) its stable evolution. (c) Unstable propagation:  $\alpha = 2, \phi_0 = 2, w_0 = 5$ ; (d) stable propagation:  $\alpha = 3, \phi_0 = 2, w_0 = 5$ . The linear-stability map of exact solitons (25) in the  $(\phi_0, w_0)$  parameter plane:  $\alpha = 2$  (e), and  $\alpha = 3$  (f), where the blue (or dark, in the black-and-white rendition) regions host stable solitons, while other regions, such as yellow and green ones (light, in the black-and-white format), are populated by unstable solitons. The nonlinearity coefficient is  $g = 1$  here.

### 3.1 1D solitons and stability

#### 3.1.1 Analytical solitons and the linear stability

Particular solutions of one-dimensional equation (4) with the Kerr nonlinearity and  $\mathcal{PT}$ -symmetric GS-II potential (19), subject to constraint Eq. (20), can be found, for the propagation constant  $\mu = \alpha^2$ , as

$$\phi(x) = \phi_0 \operatorname{sech}^\alpha x \exp\left(\frac{iw_0}{3\alpha} \int_0^x \operatorname{sech}^\alpha s ds\right). \quad (25)$$

It is worthy to note that  $\phi(x) \in \wp(\mathbb{R})$  and local intensity  $|\phi(x)|^2 = \phi_0^2 \operatorname{sech}^{2\alpha} x$  of these exact solutions depends only on  $\phi_0$  and  $\alpha$ , while the gain-loss strength  $w_0$  does not appear in the solution.

Next, we focus on the analysis of the exact nonlinear localized mode (25) in two cases, as follows.

*Case 1.* At  $\alpha = 1$ , the  $\mathcal{PT}$ -symmetric GS-II potential (19) turns into the remarkable Scarf-II potential,

$$V(x) = v_0 \operatorname{sech}^2 x, \quad W(x) = w_0 \operatorname{sech} x \tanh x, \quad (26)$$

with  $v_0 = v_1 + v_2 = w_0^2/9 - g\phi_0^2 + 2$ . Then, soliton (25) of Eq. (4) with  $\mu = 1$  becomes [86]

$$\phi(x) = \sqrt{A/g} \operatorname{sech} x e^{iw_0 \tan^{-1}(\sinh x)/3}, \quad A = \left(w_0^2/9 - v_0 + 2\right), \quad gA > 0. \quad (27)$$



- For the focusing Kerr nonlinearity ( $g = 1$ ), the soliton (25) is  $\phi(x) = \sqrt{A} (\operatorname{sech}x) \exp [(iw_0/3) \tan^{-1}(\sinh x)]$  [7].
- For the defocusing case ( $g = -1$ ), the soliton (25) becomes  $\phi(x) = \sqrt{-A} \operatorname{sech} \exp [(iw_0/3) \tan^{-1}(\sinh x)]$  [8].

*Case 2.* At  $\alpha > 0$  with  $\alpha \neq 1$ , the proposed  $\mathcal{PT}$ -symmetric GS-II potential (19) essentially extends the original Scarf-II potential, and the width of the corresponding bright soliton (25) changes. As  $0 < \alpha < 1$ , the width becomes larger, while as  $\alpha > 1$  it is smaller.

To facilitate the consideration, we start our analysis for  $\alpha = 2$  as the reference value. Under the GS-II potential (19) in Fig. 1(a), a representative exact ground-state soliton with one hump is produced by Eq. (25) (see Fig. 2(a)). We have found that, for the strength of the gain-loss distribution  $w_0 = 3$ , the soliton is stable in long direct simulations with 2% white noise added to the soliton, see Fig. 2(b). If this parameter increases to  $w_0 = 5$ , exceeding a certain threshold value, the exact nonlinear mode (25) becomes unstable, quickly spreading out in the simulations, see Fig. 2(c). This result is naturally explained by the fact that too large gain-loss force is adverse to the stability of the soliton. However, in this case, the exact soliton (25) regains its stability again for  $\alpha = 3$ , see Fig. 2(d). In fact, the growth of  $\alpha$  makes the potential well deeper, thus helping to stabilize the soliton.

To further confirm these results, the linear-stability analysis can be utilized to seek for a region where the solitons is stable is located in the  $(\phi_0, w_0)$  parameter plane. Accordingly, the linear stability is determined by the largest absolute value of imaginary parts of the eigenvalue  $\nu$  in Eqs. (25) and (17), and the logarithmic scale is used, displaying the results in the form of  $\lg[\max |\Im(\nu)|]$ . At  $\alpha = 2$  and 3, we thus find a broad blue area of stable solitons, which is shown in Figs. 2(e,f). Note that the soliton-stability area expands as  $\alpha$  increases. For example, point  $(\phi_0, w_0) = (2, 5)$  falls in the unstable region for  $\alpha = 2$ , belonging to the stability region for  $\alpha = 3$ , which explains the propagation picture plotted in Figs. 2(c,d). Further, one can observe in Fig. 2(e) that, if  $\phi_0 = 2$  is fixed, the linear-stability threshold is  $w_0 \approx 4.6$ , below which all the exact solitons are stable. This conclusion agrees well with the findings presented in Figs. 2(b,c).

By comparing Figs. 2(e) and 1(b), we conclude that the presence of the self-focusing Kerr nonlinearity can further extend the range of fully real spectra in the  $\mathcal{PT}$ -symmetric GS-II potential (19). In other words, the stability range of the localized modes can be broadened with the help of the appropriate nonlinearity. For instance, in Fig. 2(e) we observe a stable soliton under the action of the Kerr nonlinearity at  $(\phi_0, w_0) = (2, 4)$ , while the  $\mathcal{PT}$  symmetry is broken in the corresponding linear system, see Fig. 1(b).

Furthermore, the power flow (Poynting vector) associated with the nonlinear localized mode (25) is

$$S(x) = \frac{i}{2}(\phi\phi_x^* - \phi^*\phi_x) = \frac{\phi_0^2 w_0}{3\alpha} \operatorname{sech}^{3\alpha} x. \quad (28)$$

It can be seen that its positive or negative sign is solely determined by the sign of the gain-loss strength  $w_0$ . Thus, at  $w_0 > 0$ , the power always flows from the gain to loss region, as usual. In addition, at  $\alpha = 2$ , the total power of the exact nonlinear mode (25) is

$$P = \int_{-\infty}^{+\infty} |\psi(x, z)|^2 dx = \frac{4}{3} \phi_0^2. \quad (29)$$

### 3.1.2 Propagation patterns of solitons under perturbations

Another natural question concerning the dynamics of the solitons is their motion initiated by a shift,  $x \rightarrow x - x_0$ , of the exact soliton (25) from the equilibrium position, i.e., taking the initial condition as

$$\check{\phi} = \phi_0 \operatorname{sech}^\alpha(x - x_0) \exp\left(\frac{iw_0}{3\alpha} \int_0^{x-x_0} \operatorname{sech}^\alpha s ds\right). \quad (30)$$

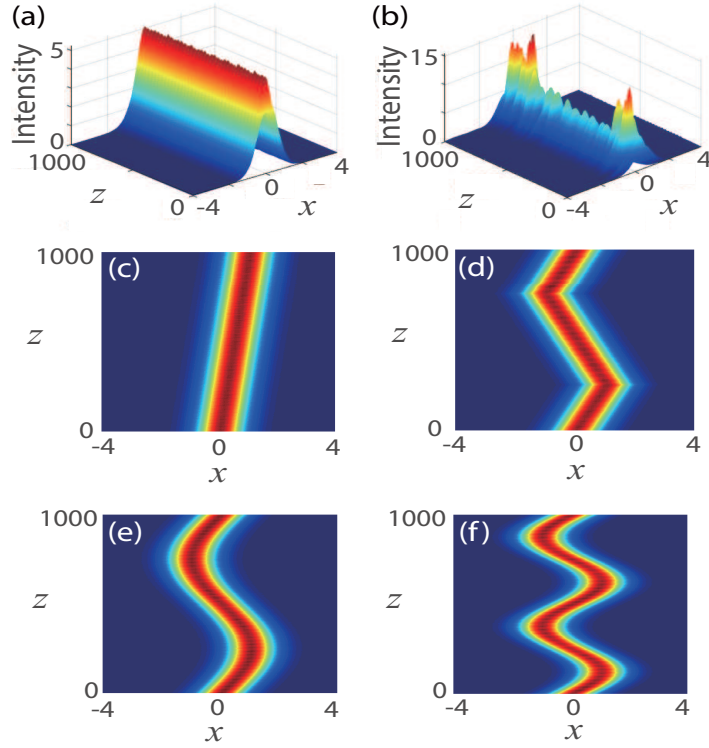


Figure 3: The propagation of nonlinear mode (25) initially shifted by  $x_0 = 0.1$  (a), or  $x_0 = 0.5$  (b). Perturbed propagation patterns of nonlinear mode (25) for different GS-II potentials (25): (c)  $\tilde{x}_0(z) = z/z_{\max}$ , (d)  $\tilde{x}_0(z)$  determined by Eq. (31), (e)  $\tilde{x}_0(z) = \sin(2\pi z/z_{\max})$ , (f)  $\tilde{x}_0(z) = \sin(4\pi z/z_{\max})$ . Other parameters are  $g = 1, \alpha = 2, \phi_0 = 2, w_0 = 3$ .

As a result, we have found that only for sufficiently small  $x_0$ , such as  $x_0 = 0.1$ , the soliton remain stable in the course of long propagation, as shown in Fig. 3(a). For larger  $x_0$ , such as  $x_0 = 0.5$ , the initially shifted soliton becomes unstable, see Fig. 3(b).

A related question is a possibility to control the transmission of the beam by making the transverse position of the potential well be a function of the propagation distance. To this end, we modify the GS-II potential given by Eqs. (19) and (20) with  $x \rightarrow x - \tilde{x}_0(z)$ . In this context, we consider linear and periodic functions for  $\tilde{x}_0(z)$ .

- The linear shift: for  $\tilde{x}_0(z) = z/z_{\max}$ , where  $z_{\max}$  is the maximum of the propagation distance, the accordingly perturbed soliton (25) propagates stably along a straight line from the original position, as shown in Fig. 3(c). If  $\tilde{x}_0(z)$  is chosen as a piecewise-linear function,

$$\tilde{x}_0(z) = \begin{cases} \frac{4z}{z_{\max}}, & 0 \leq 4z \leq z_{\max}, \\ 2 - \frac{4z}{z_{\max}}, & z_{\max} < 4z \leq 3z_{\max}, \\ \frac{4z}{z_{\max}} - 4, & 3z_{\max} < 4z \leq 4z_{\max}, \end{cases} \quad (31)$$

the soliton propagates stably in the potential given by Eqs. (19) and (20) with  $x \rightarrow x - \tilde{x}_0(z)$ , regardless of the unsmoothness of the modulation pattern (31), see Fig. 3(d).

- Under the action of the periodic shift,  $\tilde{x}_0(z) = \sin(2\pi z/z_{\max})$ , or one with the double frequency,  $\tilde{x}_0(z) = \sin(4\pi z/z_{\max})$ , the accordingly perturbed soliton (25) maintains stable snaking transmission, see Figs. 3(e)

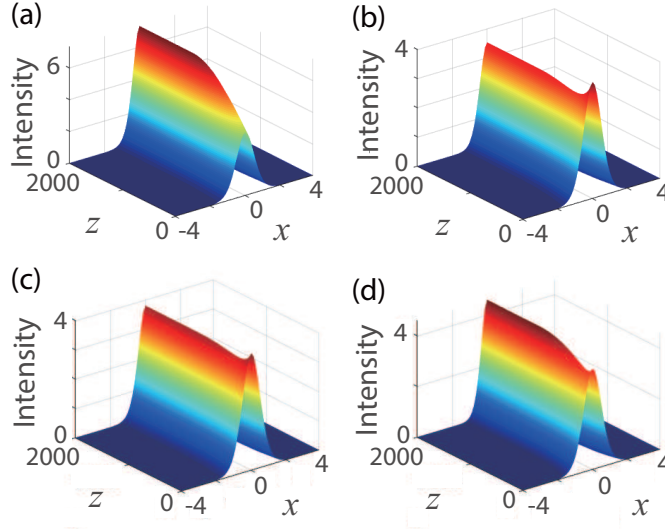


Figure 4: The application of the adiabatic transformation (33) to the nonlinear mode (25) with initial parameters  $\alpha_1 = 2, (\phi_0)_1 = 2, (w_0)_1 = 3$ : (a)  $(w_0)_1 = 3 \rightarrow (w_0)_2 = 5$ ; (b)  $\alpha_1 = 2 \rightarrow \alpha_2 = 3$ ; (c)  $(\phi_0)_1 = 2 \rightarrow (\phi_0)_2 = 1$ ; (d) the joint action of the excitations in (a), (b) and (c).

and 3(f).

Thus, it is possible to conclude that the soliton keeps its stability in the spatially modulated potential, with the soliton's center staying close to the midpoint of the moving potential well.

### 3.1.3 The adiabatic excitations of nonlinear modes

Here we address the case when the central position of the GS-II potential (19) is fixed at the origin, aiming to generate additional stable solitons from input given by Eq. (25) by varying parameters of the potential well adiabatically as functions of the propagation distance, namely,  $\alpha \rightarrow \alpha(z)$ ,  $\phi_0 \rightarrow \phi_0(z)$  or  $w_0 \rightarrow w_0(z)$ , cf. Ref. [15]. Accordingly, Eq. (1) with the  $\mathcal{PT}$ -symmetric GS-II potential (19) is replaced by

$$i \frac{\partial \psi}{\partial z} + \left[ \frac{\partial^2}{\partial x^2} + V(x, z) + iW(x, z) + |\psi|^2 \right] \psi = 0, \quad (32)$$

where the  $z$ -dependent potentials  $V(x, z)$  and  $W(x, z)$  are given by Eqs. (19) and (20) with  $\alpha \rightarrow \alpha(z)$ ,  $\phi_0 \rightarrow \phi_0(z)$  and  $w_0 \rightarrow w_0(z)$ . Here, three scenarios of the adiabatic variation of parameters  $\alpha(z)$ ,  $\phi_0(z)$  and  $W_0(z)$  are chosen in the form of

$$\Xi(z) = \begin{cases} (\Xi_2 - \Xi_1) \sin\left(\frac{\pi z}{z_{\max}}\right) + \Xi_1, & 0 \leq z < z_{\max}/2, \\ \Xi_2, & z \geq z_{\max}/2, \end{cases} \quad (33)$$

where  $\Xi_{1,2}$  denote the initial and final values.

First, we apply the single-parameter variation to the bright soliton (25), which is taken as the initial condition, and its propagation is governed by Eq. (32). When  $w_0(z)$  is replaced with  $\Xi(z)$  given by Eq. (33), whereas  $\alpha(z) \equiv \alpha$  and  $\phi_0(z) \equiv \phi_0$  are fixed, we can adiabatically transform the initially stable localized mode produced by Eq. (25) at  $(\alpha, \phi_0, (w_0)_1) = (2, 2, 3)$  to another stable mode corresponding to parameters  $(\alpha, \phi_0, (w_0)_2) = (2, 2, 5)$ , see Fig. 4(a), even if the corresponding linear  $\mathcal{PT}$ -symmetry is broken [see Fig. 1(b)] and the corresponding exact soliton (25)

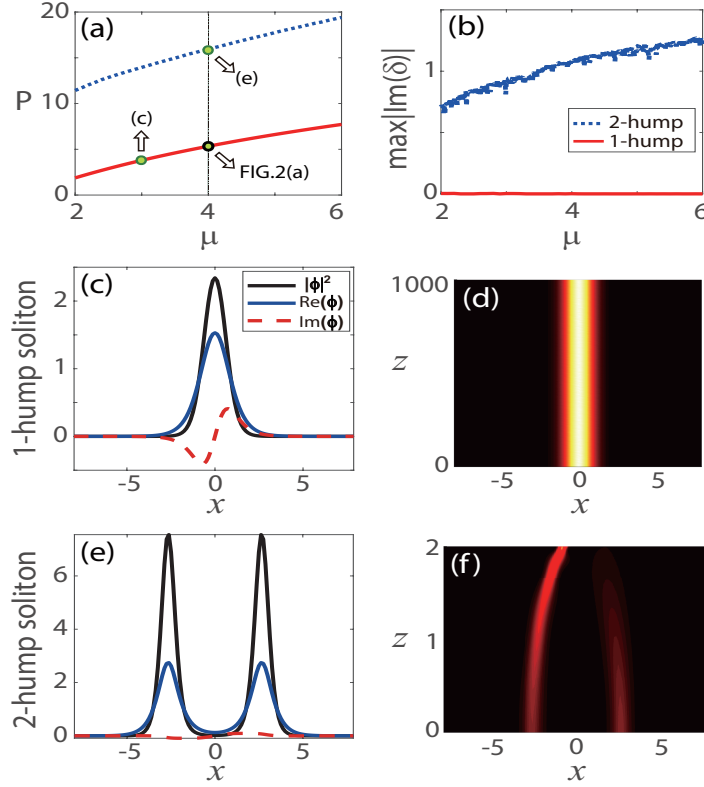


Figure 5: (a) The power and (b) the corresponding linear-stability versus the propagation constant  $\mu$ , for the fundamental (1-hump) and first-excited-state (2-hump) solitons, produced by numerical methods. The numerically found solitons and their propagation: (c,d) for  $\mu = 3$  (fundamental soliton), (e,f)  $\mu = 4$  (first-excited-state soliton). Other parameters are  $g = 1, \alpha = 2, \phi_0 = 2, w_0 = 3$ .

is unstable [see Fig. 2(c)]. This is an unexpected result, since the stability of the transformed soliton should in general remain consistent with that of the exact soliton (25) for the same parameters.

Replacing parameter  $\alpha(z)$  or  $\phi_0(z)$  by expression Eq. (33) and keeping the other parameters unchanged, similar transformations of soliton (25) can be executed as well. As a result, non-monotonous adiabatic-transform scenarios are observed in Figs. 4(b, c). It is worthy to note that in Fig. 4(c) we need to make the value of  $(\phi_0)_2$  smaller than  $(\phi_0)_1 = 2$ , to produce the stable adiabatic transform. Otherwise, the potential parameters in the final state, such as, e.g.,  $(\alpha, (\phi_0)_2, w_0) = (2, 3, 3)$ , will make the soliton (25) unstable [see Fig. 2(e)], destabilizing the entire procedure.

Next, the simulations demonstrate that the adiabatic transformation remains stable if the substitution (33) is applied to all the three parameters under the consideration,  $(\alpha, \phi_0, w_0)$ . In this case, Fig. 4(d) shows that the result of the simultaneous variation of the three parameters seems as a superposition of the results produced by the single-parameter variations. Thus, the exact soliton (25) can be stably transformed to another nonlinear mode by the properly applied adiabatic variation of the potential's parameters.

### 3.1.4 Internal modes and high-order solitons

The preceding analysis is focused on exact solitons (25) of Eq. (4) with  $\mu = \alpha^2$ . It is, however, natural to expect that Eq. (4) may produce other modes for different values of  $\mu$ . They can be produced by means of the iteration

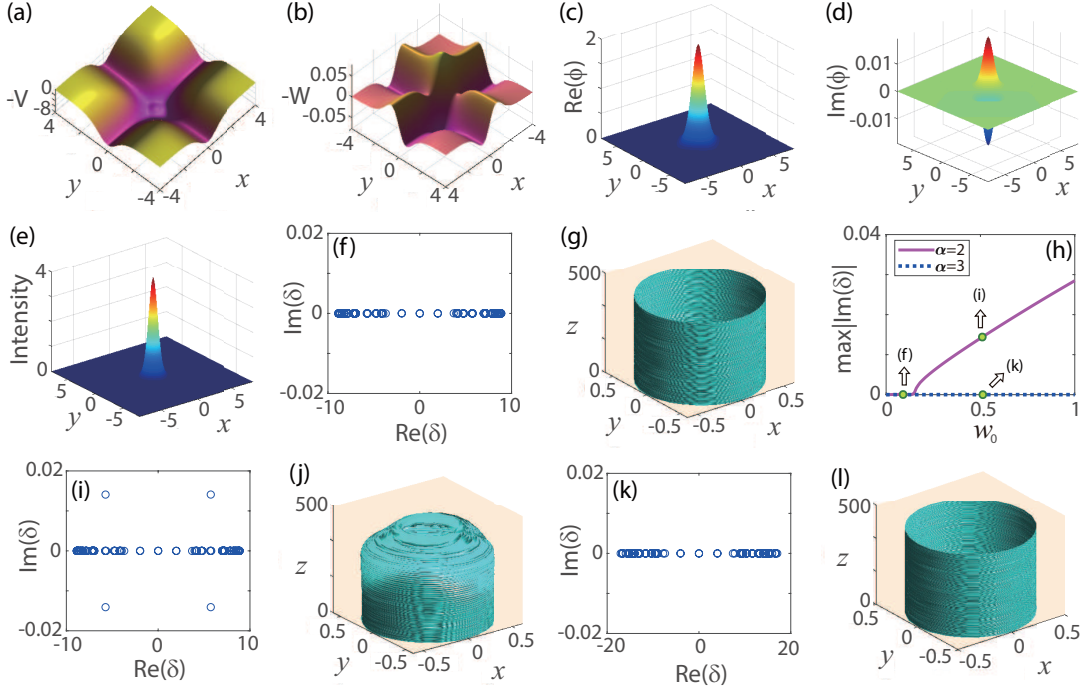


Figure 6: (color online). (a,b) Real and imaginary components of the 2D  $\mathcal{PT}$ -symmetric generalized Scarf-II potential,  $U = -V(x, y) - iW(x, y)$ , with  $(\alpha, \phi_0, w_0) = (2, 2, 0.1)$ , (c,d,e) Real and imaginary parts and intensity of the corresponding 2D exact soliton. (f) The linear stability spectrum of the soliton. (g) The stable propagation. (h) The change of the linear-stability index as a function of  $w_0$ , at  $\alpha = 2$  and 3. The linear stability spectrum and propagation of the 2D exact solitons are displayed at  $\alpha = 2, w_0 = 0.5$  (i,j);  $\alpha = 3, w_0 = 0.5$  (k,l). Other parameters are  $g = 1$ .

scheme developed in Sec. 2.3. To this end, we choose a Gaussian input,

$$\phi_{\text{ini}}(x) = \rho |x|^m e^{-w^{-2}x^2}, \quad m \in \mathbb{Z}^+ \quad (34)$$

with real amplitude  $\rho$  and width  $w$ . The iteration scheme (15) demonstrates that the initial Gaussian (34) converges to the exact soliton (25) with  $\mu = \alpha^2$ . For instance, at  $\alpha = 2$ , hence  $\mu = 4$ , we numerically obtain a localized nonlinear mode which is identical to the exact soliton (25), marked by the black circle in Fig. 5(a). For values of  $\mu$  close to 4, with fixed  $\alpha = 2$ , we can take soliton (25) at  $\mu = 4$  as the input, so as to improve the convergence speed of the numerical scheme and produce a family of solitons (fundamental modes) shown by the solid red line in Fig. 5(a), as a function of  $\mu$ . At  $\mu = 3$ , a representative fundamental mode is exhibited in Fig. 5(c). The wave propagation is stable in a long time, see Fig. 5(d).

On the other hand, we can produce families of higher-order nonlinear modes by means of the modified squared-operator iteration method [82]. In particular, the generated family of the first excited states is plotted by the blue dotted line in Fig. 5(a). A typical soliton representing the first excited state (see Fig. 5(e)) turns out to be unstable in direct simulations (see Fig. 5(f)).

Linear-stability plots for the ground and first excited states are presented in Fig. 5(b). It is seen that the ground states are completely stable, however the first excited states are unstable, in agreement with Figs. 5(d,f). It has been checked that excited states of higher orders are subject to a still stronger instability.

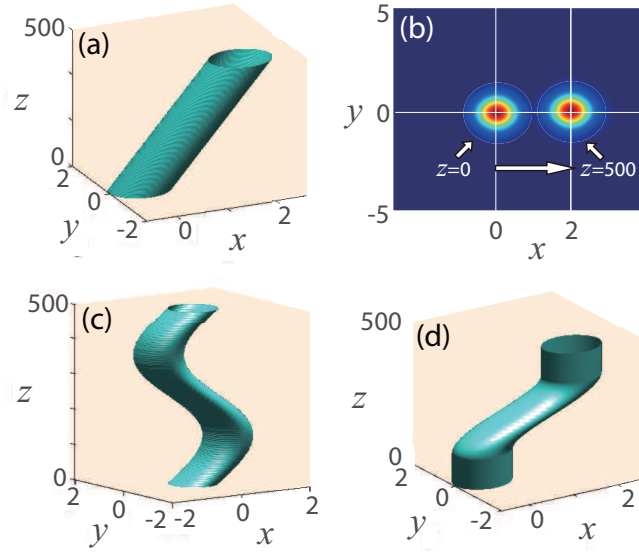


Figure 7: Evolution patterns of the 2D soliton (36) for different modulation patterns of the GS-II potential (22) with  $x_j - \bar{x}_{j0}(z)$ : (a)  $\bar{x}_{10}(z) = 2z/z_{\max}$ ; (b) the respective initial and final states; (c)  $\bar{x}_{10}(z) = \sin(2\pi z/z_{\max})$ ; (d) for  $\bar{x}_{10}(z)$  given by Eq. (38). Other parameters are  $g = 1$ ,  $\alpha = \phi_0 = 2$ ,  $w_0 = 0.1$ .

## 3.2 2D solitons and stability

### 3.2.1 Exact spatial solitons

In this section, we address the formation of 2D spatial solitons and their stability in the 2D geometry determined by the  $\mathcal{PT}$ -symmetric GS-II potential defined by Eqs. (22) and (23) (see Figs. 6(a,b)). In this case, Eq. (1) becomes

$$i\frac{\partial\psi}{\partial z} + \nabla_2^2\psi + [V(x,y) + iW(x,y)]\psi + g|\psi|^2\psi = 0, \quad (35)$$

with  $\nabla_2 = (\partial_x, \partial_y)$ . Then, an exact localized solution of Eq. (35) is sought for as

$$\psi = \phi_0(\operatorname{sech}x \operatorname{sech}y)^\alpha \exp\left(2i\alpha^2 z + \frac{iw_0}{3\alpha} \sum_{x_j=x,y} \int_0^{x_j} \operatorname{sech}^\alpha s ds\right). \quad (36)$$

The stationary solution  $\phi(x,y)$  is exhibited by its real and imaginary components, as well as intensity  $|\phi(x,y)|^2$ , in Figs. 6(c,d,e). The linear-stability spectrum without any imaginary parts in Fig. 6(f) reveals that this stationary soliton is stable. Direct propagation simulations of this 2D soliton further confirm its stability, as shown by contour lines of the soliton intensity,  $(1/2) \max(|\psi(x,y,0)|^2)$ , in Fig. 6(g). Moreover, the solid curve in Fig. 6(h) shows that the 2D modes are linearly stable only below the critical value, i.e., at  $w_0 < (w_0)_{\text{crit}} \approx 0.15$ , while other parameters are fixed. For instance, the above-mentioned 2D soliton (36) is indeed stable, as it was found for  $w_0 = 0.1 < (w_0)_{\text{crit}}$ , while the increase of  $w_0$  to 0.5 makes the 2D soliton unstable, as shown by its linear-stability spectrum and nonlinear propagation, see Figs. 6(i,j). However, the blue dotted line in Fig. 6(h) shows that the increase of  $\alpha$  to 3 makes the 2D modes linearly stable in a broader range of  $w_0$ , as is corroborated by Figs. 6(k,l).

### 3.2.2 The evolution of 2D spatial solitons under perturbations and excitation

When the 2D GS-II potential well (22) varies along the propagation distance, the governing 2D model becomes

$$i\frac{\partial\psi}{\partial z} + \left[ \nabla_2^2 + V(x, y, z) + iW(x, y, z) + |\psi|^2 \right] \psi = 0. \quad (37)$$

Like the 1D case, the first issue to address is the possibility of stable propagation of the soliton initiated by solution (36) when the central position of the 2D GS-II potential (22) depends on the propagation distance, that is, we considered the potential  $V(x, z)$  and  $W(x, z)$  given by Eq. (22) with  $x_j - \tilde{x}_{j0}(z)$ , where we set  $\tilde{x}_{j0}(0) = 0$  to make the 2D nonlinear mode (36) a correct solution of Eq. (37) under the GS-II potential (22) at  $z = 0$ .

Here, we always set  $\tilde{x}_{20}(z) = 0$  and consider three options for  $\tilde{x}_{10}(z)$ , as follows:

- The linear perturbation: When the central position of the 2D GS-II potential (22) with  $x_j - \tilde{x}_{j0}(z)$  uniformly moves to the right in the  $x$  direction with the growth of the propagation distance, such as  $\tilde{x}_{10}(z) = 2z/z_{\max}$ , the soliton propagates stably along the same  $x$  direction, as is shown in Fig. 7(a). In particular, Fig. 7(b) clearly indicates the central position of the 2D soliton in the initial and final states.
- The periodic perturbation: When the central position of the 2D GS-II potential (22) with  $x_j - \tilde{x}_{j0}(z)$  oscillates periodically in the  $x$  direction as a function of the propagation distance, i.e.,  $\tilde{x}_{10}(z) = \sin(2\pi z/z_{\max})$ , the soliton initiated by Eq. (36) demonstrates stable snaking propagation, see Fig. 7(c). In this case, the final central position of the 2D soliton is the same as the initial one, both being at the origin. The same result is true for the periodic modulation with the double frequency,  $\tilde{x}_{10}(z) = \sin(4\pi z/z_{\max})$ .
- A mixed perturbation: When the path  $\tilde{x}_{10}(z)$  is taken as the following piecewise function.

$$\tilde{x}_{10}(z) = \begin{cases} 0, & 0 \leq z \leq \frac{z_{\max}}{4}, \\ \sin\left(\frac{2\pi z}{z_{\max}} - \pi\right) + 1, & \frac{z_{\max}}{4} < z \leq \frac{3z_{\max}}{4}, \\ 2, & \frac{3z_{\max}}{4} < z \leq z_{\max}, \end{cases} \quad (38)$$

the soliton also moves stably, staying trapped in the potential well (22) with  $x_j - \tilde{x}_{j0}(z)$ , in spite of the presence of inflection points, see Fig. 7(d).

Thus, similar to the 1D case, the stable 2D nonlinear mode (36) propagates in the robust form along the trajectory determined by the central position of potential well (22) with  $x_j - \tilde{x}_{j0}(z)$ .

Another issue is whether it is possible to transform the stable 2D soliton by adiabatically altering the potential's parameters. For this purpose, similar to the 1D case, we make the potential-well parameters  $(\alpha, \phi_0, w_0)$  in Eq. (22) varying, i.e.,  $\alpha \rightarrow \alpha(z)$ ,  $\phi_0 \rightarrow \phi_0(z)$  and/or  $w_0 \rightarrow w_0(z)$ .

Here we consider the case of the switch of  $\alpha(z)$  in the form of Eq. (33) and  $\phi_0(z) \equiv \phi_0$ ,  $w_0(z) \equiv w_0$ . More specifically, taking  $\phi_0(z) \equiv 2$ ,  $w_0(z) \equiv 0.5$ , and

$$\alpha(z) = \begin{cases} \sin(\pi z/z_{\max}) + 2, & 0 \leq z < z_{\max}/2, \\ 3, & z \geq z_{\max}/2, \end{cases} \quad (39)$$

we start with an initially unstable 2D soliton (36) at  $(\alpha, \phi_0, w_0) = (2, 2, 0.5)$ , transforming it into another *stable* localized mode with parameters  $(\alpha, \phi_0, w_0) = (3, 2, 0.5)$ , as shown by contours and profiles in Figs. 8(a,b). Here, Fig. 8(c) displays the initial unstable soliton [see Fig. 6(j)], while Fig. 8(d) exhibits the stable final-state soliton. It

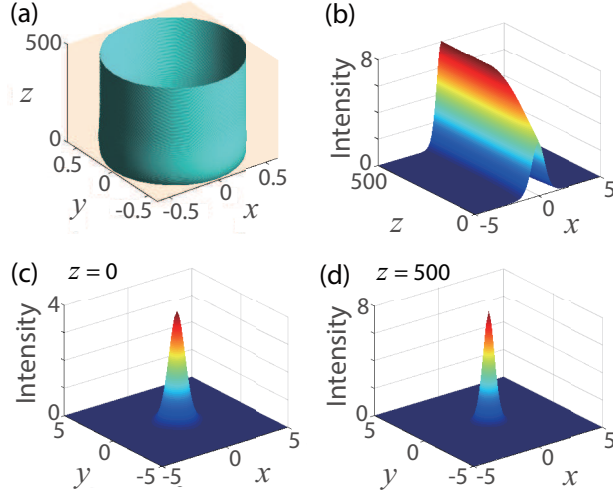


Figure 8: The transformation of the 2D nonlinear mode (36) in Eq. (37) with the potential well (22) in which  $\alpha \rightarrow \alpha(z)$ ,  $\phi_0 \rightarrow \phi_0(z)$  and/or  $w_0 \rightarrow w_0(z)$ : (a) the contour plot of the intensity of the nonlinear mode; (b) the corresponding propagation in the  $y = 0$  cross section; (c) the initial-state soliton; (d) the final-state soliton. Here  $\alpha(z)$  is given by Eq. (39) and other parameters are  $g = 1, \phi_0 = 2, w_0 = 0.5$ .

is worthy to note that the final-state soliton is a new nonlinear mode whose shape (with the peak value  $\phi_{\max}^2 \approx 8$ ) is conspicuously different from that of the exact 2D soliton (36) at  $(\alpha, \phi_0, w_0) = (3, 2, 0.5)$ , whose peak intensity is  $\phi_{\max}^2 = 4$ .

Thus, the 2D exact soliton (36) can be stably transformed to other nonlinear localized modes, like in the 1D case, by means of the adiabatic variation of the parameters of the GS-II potential (22) with  $\alpha \rightarrow \alpha(z)$ ,  $\phi_0 \rightarrow \phi_0(z)$  and/or  $w_0 \rightarrow w_0(z)$ .

### 3.2.3 2D internal modes and high-order solitons

Once the parameters of the 2D system (35) and GS-II potential (22) with  $\alpha \rightarrow \alpha(z)$ ,  $\phi_0 \rightarrow \phi_0(z)$  and/or  $w_0 \rightarrow w_0(z)$  are fixed as per Eq. (36), we obtain the single exact fundamental mode corresponding to  $\mu = 2\alpha^2$ . Varying parameter  $\mu$ , other nonlinear localized modes can be found, including 2D fundamental solitons.

To address this possibility, we start with the potential's parameters  $(\alpha, \phi_0, w_0) = (2, 2, 0.1)$ . By means of the numerical iteration technique developed in Sec. 2.3 and taking the exact 2D soliton at  $\mu = 8$  as the input, a family of new 2D fundamental solitons can be found with values of the propagation constant around  $\mu = 8$ , as shown by the solid blue line in Fig. 9(a). Figure 9(a) also plots the power curve of the 2D fundamental solitons, with  $w_0 = 0.5$ , by the red dotted line, which is the same as the one of the 2D fundamental solitons with  $w_0 = 0.1$ . This result is reasonable because, at least for  $\mu = 8$ , we see from Eq. (36) that the exact 2D fundamental solitons do not change their density as  $w_0$  varies.

However, the linear-stability analysis, as shown in Fig. 9(b), reveals that the stability of these two families of solitons is very different. The first family, with  $w_0 = 0.1$ , is entirely stable, while the family with  $w_0 = 0.5$  is partially unstable, especially near  $\mu = 8$ . This happens because the growth of  $w_0$  increases the strength of the gain-loss distribution, which easily leads to instability of the soliton. Although the family of solitons with  $w_0 = 0.5$  is unstable near  $\mu = 8$ , we can find a series of stable modes from Fig. 9(b) by adjusting the propagation constant appropriately. For example, when  $\mu = 7$ , a 2D fundamental mode is numerically obtained and the propagation simulation confirms that it is stable [see Figs. 9(c) and (d)], which is consistent with the result of the linear-stability



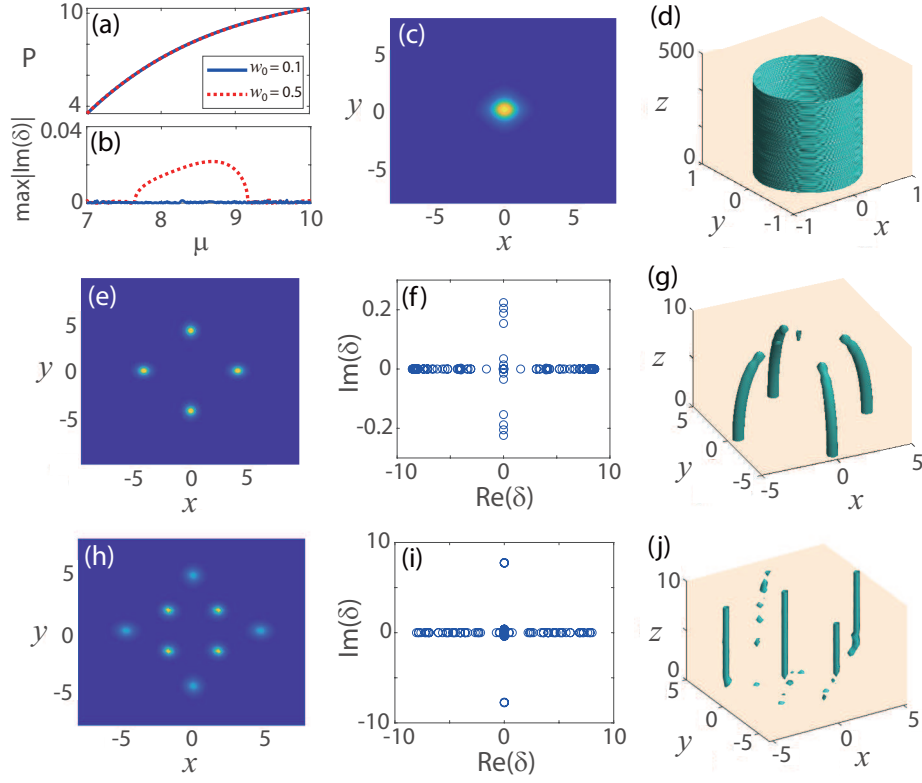


Figure 9: (color online). (a) The power and (b) the corresponding linear-stability eigenvalue of the 2D fundamental solitons versus the propagation constant  $\mu$  for  $w_0 = 0.1$  and  $0.5$ , produced by the numerical solution. (c) The numerically found fundamental soliton depicted by means of the intensity, and (d) its propagation with  $\mu = 7$ , nearby the exact solution corresponding to propagation constant  $\mu = 8$ . Higher-order vortex solitons, linear-stability spectra, and the transmission dynamics with  $w_0 = 0.1$ : (e, f, g)  $m = 1$  (4-vortex), (h, i, j)  $m = 2$  (8-vortex). Other parameters are  $g = 1, \alpha = \phi_0 = 2$ .

analysis in Fig. 9(b).

In addition, we have found that families of 2D vortex solitons exist too, but they are unstable. For instance, using the modified squared-operator iteration method with the input of the following form,

$$\phi_{\text{ini}}(x, y) = \rho (x^2 + y^2)^{m/2} \exp\left(-\frac{x^2 + y^2}{w^2}\right), \quad m \in \mathbb{Z}^+, \quad (40)$$

where amplitude  $\rho$  and width  $w$  need to be chosen appropriately, we can produce four-peak and eight-peak vortex solitons [see Figs. 9(e, h)], with winding numbers  $m = 1$  and  $2$ . The computation of their linear-stability spectrum and direct simulations clearly demonstrate that they are unstable solutions, see Figs. 9(f)-(j).

### 3.3 3D “light bullets” and their stability

#### 3.3.1 3D “light bullets”

3D spatiotemporal solitons, alias “light bullets”, are also a subject of great significance in nonlinear optics [90,91]. In this section we address the formation of 3D solitons in the 3D  $\mathcal{PT}$ -symmetric GS-II potential. The 3D governing equation with this potential and Kerr nonlinearity is written as [32]

$$i \frac{\partial \psi}{\partial z} + \left[ \nabla_3^2 + V(x, y, t) + iW(x, y, t) + g|\psi|^2 \right] \psi = 0, \quad (41)$$

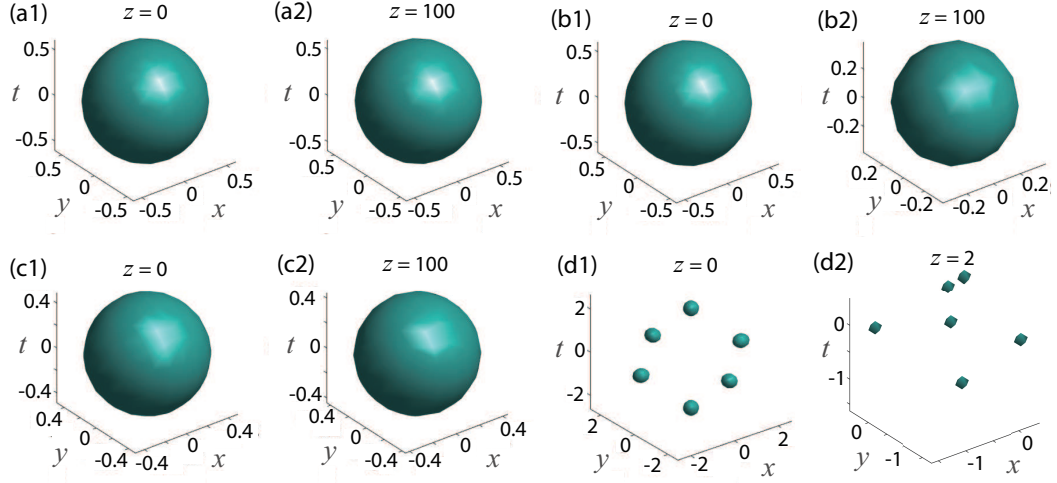


Figure 10: (color online). The isosurface evolution of 3D exact solitons (“light bullets”) with  $\mu = 3\alpha^2$ : (a1, a2)  $\alpha = 2, w_0 = 0.1$ ; (b1, b2)  $\alpha = 2, w_0 = 0.5$ ; (c1, c2)  $\alpha = 3, w_0 = 0.5$ . (d1,d2) The isosurface evolution of a higher-order “bullet” obtained numerically with the same parameters as in (a1,a2). Other parameters are  $g = 1, \phi_0 = 2$ .

with  $\nabla_3 = (\partial_x, \partial_y, \partial_t)$ ,  $V(x, y, t)$ ,  $W(x, y, t)$  given by Eqs. (24) and (23). A necessary caveat is that, unlike the 1D and 2D setting, the experimental realization of fully three-dimensional potentials in optics is quite difficult, as creating a particular potential form in the temporal direction is a challenging problem. For this reason, the results presented below for 3D solutions have a methodological interest, rather than promising direct physical implementation. On the other hand, they may be directly interpreted in terms of the Gross-Pitaevskii equation for Bose-Einstein condensates, subject to the action of the 3D  $\mathcal{PT}$ -symmetric potential (the same is possible for the 1D and 2D settings considered above) [92].

In the 3D  $\mathcal{PT}$ -symmetric GS-II potential (24), the exact 3D solution of Eq. (41) can be obtained in the stationary form,

$$\psi = \phi_0 (\text{sech}x \text{sech}y \text{sech}t)^\alpha \exp \left( 3i\alpha^2 z + \frac{iw_0}{3\alpha} \sum_{x_j=x,y,t} \int_0^{x_j} \text{sech}^\alpha s ds \right), \quad (42)$$

In particular, for  $\alpha = 1$  and  $\phi_0 = \sqrt{(w_0^2 - 9v_0 + 18)/(9g)}$  the 3D  $\mathcal{PT}$ -symmetric GS-II potential (24) reduces to

$$V = (w_0^2/9 + 2) \sum_{x_j=x,y,t} \text{sech}^2 x_j + (v_0^2 - 2 - w_0^2/9) \prod_{x_j=x,y,t} \text{sech}^2 x_j, \quad W = w_0 \sum_{x_j=x,y,t} \text{sech} x_j \tanh x_j. \quad (43)$$

and solution (42) becomes

$$\psi = \phi_0 (\text{sech}x) (\text{sech}y) (\text{sech}t) e^{i\varphi(x,y,t) + 3iz}, \quad (44)$$

with  $\varphi(x, y, t) = \frac{w_0}{3} \sum_{x_j=x,y,t} \arctan(\sinh x_j)$ , whose stability has been investigated [32].

However, for  $\alpha > 0$  and  $\alpha \neq 1$ , the 3D  $\mathcal{PT}$ -symmetric GS-II potential (24) is essentially more general than the one with  $\alpha = 1$ , which makes the corresponding 3D solution significantly more general too. Here we take  $\alpha = 2$  as an example to illustrate the stability of the analytical 3D solution (42). Fig. 10(a1) displays the isosurface plot of a typical 3D soliton with  $(\phi_0, w_0) = (2, 0.1)$ . Just as in the 2D case, the soliton exhibits stable propagation in the course of long simulations [see Fig. 10(a2)], while increasing  $w_0$  to 0.5 makes the soliton compressed after travelling a certain distance, as shown in Figs. 10(b1) and 10(b2). In this case, if the value of  $\alpha$  increases properly, the soliton again keeps its waveform unchanged and demonstrates stable propagation, see Figs. 10(c1) and 10(c2).

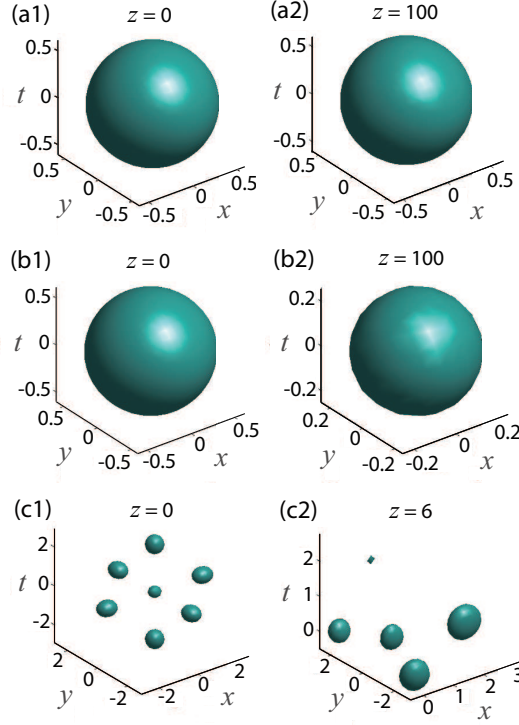


Figure 11: (color online). The isosurface evolution of 3D light bullets with  $\mu = 12$ : (a1, a2)  $w_0 = 0.1$ , (b1, b2)  $w_0 = 0.5$ , (c1, c2) The isosurface evolution of a 3D soliton with  $\mu = 10$  and  $w_0 = 0.1$ . Other parameters are  $g = 1$ ,  $\alpha = \phi_0 = 2$ .

We have also numerically investigated higher-order 3D solitons, finding that they are unstable. For instance, a higher-order six-peak soliton, produced by the numerical solution for  $(\phi_0, w_0) = (2, 0.1)$ , is displayed in Fig. 10(d1). However, it is strongly unstable and quickly collapses in the course of the propagation, see Figs. 10(d2).

### 3.3.2 $n$ -dimensional nonlinear localized mode

Finally, we further generalize the  $\mathcal{PT}$ -symmetric GS-II potential (19) to an abstract  $n$ -dimensional form,

$$V(\mathbf{x}) = \sum_{j=1}^n (v_1 \operatorname{sech}^2 x_j + v_{21} \operatorname{sech}^{2\alpha} x_j) + v_{22} \prod_{j=1}^n \operatorname{sech}^{2\alpha} x_j, \quad W(\mathbf{x}) = w_0 \sum_{j=1}^n \operatorname{sech}^\alpha x_j \tanh x_j, \quad (45)$$

where  $v_1$ ,  $v_{21}$  and  $v_{22}$  are subject, as above, to constraint (23). By means of the analysis similar to that developed above in subsection Sec. (2.1), one can readily find that Eq. (1) admits a particular exact soliton solution of the following stationary form:

$$\psi = \phi_0 \prod_{j=1}^n \operatorname{sech}^\alpha x_j \exp \left( i n \alpha^2 z + \frac{i w_0}{3\alpha} \sum_{j=1}^n \int_0^{x_j} \operatorname{sech}^\alpha s \, ds \right). \quad (46)$$

With the help of the aforementioned numerical method, one can verify that it is indeed a correct  $n$ -dimensional solution.

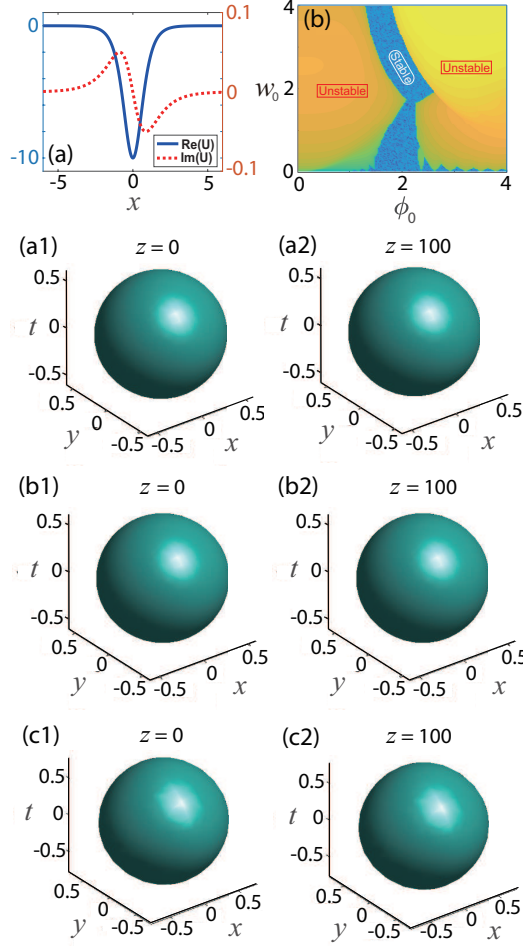


Figure 12: (color online). 3D solutions under the action of the self-defocusing nonlinearity,  $g = -1$ . (a) Real and imaginary parts of the  $\mathcal{PT}$ -symmetric GS-II potential  $U = -V(x) - iW(x)$  with  $w_0 = 0.1$ . (b) The linear-stability map of exact solitons (25) in the  $(\phi_0, w_0)$  plane. The isosurface evolution of 3D exact solutions with  $\mu = 12$ : (a1,a2)  $w_0 = 0.1$ ; (b1,b2)  $w_0 = 0.5$ . (c1,c2): The isosurface evolution of the 3D soliton with  $\mu = 10$  and  $w_0 = 0.1$ . Other parameters are  $\alpha = \phi_0 = 2$ .

## 4. Multi-dimensional solitons in an alternative $\mathcal{PT}$ -symmetric GS-II potential

### 4.1 The second $n$ -dimensional GS-II potential and an exact solution

In this section, we briefly consider another form of a  $\mathcal{PT}$ -symmetric GS-II potential in  $n$  dimensions and the corresponding solutions for localized modes. To this end, the  $n$ -dimensional  $\mathcal{PT}$ -symmetric GS-II potential (45) is replaced by the following form:

$$V(\mathbf{x}) = v_1 \sum_{j=1}^n \operatorname{sech}^2 x_j + v_2 \prod_{j=1}^n \operatorname{sech}^{2\alpha} x_j, \quad W(\mathbf{x}) = w_0 \sum_{j=1}^n \operatorname{sech} x_j \tanh x_j, \quad (47)$$

where  $v_1, v_2$  and  $w_0$  are real parameters. If one considers the constraints of  $v_1, v_2, w_0$  as

$$v_1 = \alpha(\alpha + 1) + w_0^2 / (2\alpha + 1)^2, \quad v_2 = -g\phi_0^2, \quad (48)$$

one can readily find that Eq. (1) possesses the exact stationary solution:

$$\psi(\mathbf{x}, z) = \phi_0 e^{i\varphi(\mathbf{x}) + in\alpha^2 z} \prod_{k=1}^n \operatorname{sech}^\alpha x_k, \quad \varphi(\mathbf{x}) = \frac{w_0}{2\alpha + 1} \sum_{k=1}^n \tan^{-1}(\sinh x_k). \quad (49)$$

where both  $\alpha$  and  $\phi_0$  are real potential parameters, as above.

If  $\alpha = 1$ , the GS-II potential (47), subject to constraint (48), is tantamount to the above GS-II potential defined by Eqs. (45) and (23). Accordingly, the exact nonlinear mode (49) is tantamount to one given above by Eq. (46). On the other hand, the present  $n$ -dimensional GS-II potential (47) and exact mode (49) generalize results reported in Ref. [86], where 1D and 2D spatial solitons and their stability were investigated in detail. Next we aim to elaborate the formation and propagation of solitons in the 3D  $\mathcal{PT}$ -symmetric GS-II potential (47) under the action of self-focusing and defocusing cubic nonlinearity.

## 4.2 Stability of the 3D light bullets

In the 3D case ( $n = 3$ ), the exact solution can be generated by Eq. (49) and stay stable within a certain range of the potential's parameters. More explicitly, setting  $(x_1, x_2, x_3) = (x, y, t)$ , the 3D GS-II potential becomes

$$\begin{aligned} V &= [\alpha(\alpha + 1) + w_0^2/(2\alpha + 1)^2] \sum_{x_j=x,y,t} \operatorname{sech}^2 x_j - g\phi_0^2 \prod_{x_j=x,y,t} \operatorname{sech}^{2\alpha} x_j, \\ W &= w_0 \sum_{x_j=x,y,t} \operatorname{sech} x_j \tanh x_j. \end{aligned} \quad (50)$$

With this potential, Eq. (49) yields the following exact solution:

$$\psi = \phi_0 [(\operatorname{sech} x) (\operatorname{sech} y) (\operatorname{sech} t)]^\alpha e^{i\varphi(x,y,t) + 3i\alpha^2 z}, \quad \varphi(x, y, t) = \frac{w_0}{2\alpha + 1} \sum_{x_j=x,y,t} \arctan(\sinh x_j). \quad (51)$$

For  $w_0 = 0.1$ , Fig. 11(a1) displays a representative 3D exact solution, which is depicted by means of its isosurface. The solution is stable, keeping its profile in the course of the the propagation up to  $z = 100$ , see Fig. 11(a2). However, for  $w_0 = 0.5$  the exact solution (51) is compressed and loses its stability for a long propagation distance, as seen in Figs. 11(b1,b2). Furthermore, in a vicinity of the propagation constant corresponding to the exact 3D solution, we have found 3D higher-order solitons in the numerical form, as shown in Fig. 11(c1). However, they are subject to strong instability. For example, a short propagation distance,  $z = 6$ , is sufficient for the destruction of the higher-order mode in Fig. 11(c2), built from the input

$$\phi_{\text{ini}}(\mathbf{x}) = \rho |\mathbf{x}|^m e^{-x^2/w^2}, \quad |\mathbf{x}| = \sqrt{\sum_{i=1}^n x_i^2}. \quad (52)$$

In the case of the self-defocusing,  $g = -1$ , we have also explored solutions supported by the  $\mathcal{PT}$ -symmetric GS-II potential in the 1D and multidimensional settings. Here we only produce a brief overview of the results. What is essentially different from the case of the self-focusing,  $g = 1$ , is that the GS-II potential gets back to the single-well shape, similar to the usual Scarf-II potential, see Fig. 12(a). Then, it is easy to prove that such a potential may have entirely real linear energy spectra. It also admits exact and stable localized states, although in a relatively narrow range of the potential's parameters [see Fig. 12(b) for the 1D case]. Here we consider 3D solutions as examples. Fixing  $\phi_0 = 2$  and  $w_0 = 0.1$ , we find that the respective exact 3D localized solution propagates stably for a long distance, see Figs. 12(a1,a2). Even if increasing  $w_0$  to 0.5, the fundamental mode can retain its shape over a long propagation distance [see Figs. 12(b1,b2)]. Thus, the stability of such solutions is apparently weaker than for their counterparts with  $g = 1$  (in the case of the self-focusing). In addition, for values of the propagation constant around the exact 3D solution, we found a family of stable fundamental 3D modes in the numerical form. For instance, Fig. 12(c1) exhibits a 3D numerically found fundamental mode with  $\mu = 10$ , while Fig. 12(c2) confirms its stability, as tested by the direct simulations.

## 5. Conclusions and discussions

In this work we have constructed a class of non-Hermitian  $\mathcal{PT}$ -symmetric potentials in the  $n$ -dimensional geometry, which is a significant generalization of the classical Scarf-II potentials. In the linear regime, we have proven that the 1D GS (generalized-Scarf)-II potentials may possess purely real spectra in a certain area of the space of the potential's parameters, with  $\mathcal{PT}$ -symmetry breaking occurring at borders of this area. By carefully adjusting the localization parameter, the range of the potential's parameters corresponding to the completely real spectra can be further expanded. Similar results are obtained for multidimensional settings. In the cubic-nonlinear media,  $n$ -dimensional nonlinear localized modes are obtained in the exact analytical form. The numerically performed linear-stability analysis reveals that the exact nonlinear modes may be stable in a certain range of the potential's parameters. Properly increasing the localization parameter, one can enlarge the stability domain for the soliton solutions. Overall, the stability of the exact solutions deteriorates with the increase of dimension  $n$  or strength  $w_0$  of the the gain-loss term (the imaginary part of the  $\mathcal{PT}$ -symmetric potential). Using numerical approaches, we have constructed continuous families of fundamental and excited-state solitons. The former ones tend to be stable, while the latter solutions are subject to strong instability. These unstable modes include 1D multimodal solitons, 2D solitary vortices, and 3D multi-peak solutions. By means of adiabatic modulations of the GS-II potential, the transformation of the solutions into exact solitons can be performed. We have also demonstrated that stable solitons can always propagate stably, being trapped in a slowly moving potential well, which may be used for various manipulations of the optical solitons. Finally, we have presented another category of  $n$ -dimensional  $\mathcal{PT}$ -symmetric GS-II potentials and the corresponding analytical solutions for localized 3D modes, which may be stable in the model with both self-focusing and defocusing signs of the Kerr (cubic) nonlinearity.

Lastly, we note that analytical and numerical methods developed in the present work can be applied to more general NLS-like equations, with other types of  $\mathcal{PT}$ -symmetric potentials or more complex nonlinearities. In 1D, they may be written as

$$i\frac{\partial\psi}{\partial z} = \sum_{k=1}^m c_k(x)p^k\psi + [V(x) + iW(x)]\psi - g(x)\hat{N}[\psi, \psi_x, |\psi|^2, (|\psi|^2)_x, \dots], \quad (53)$$

where  $\psi \equiv \psi(x, z)$  is the complex-valued wave function,  $p = -i\partial/\partial x$  is the momentum operator,  $c_k(x)$  and  $g(x)$  are real even functions of coordinate  $x$ , assuming that  $c_2(x)$  is positive-definite, while both the potential  $V(x) + iW(x)$  and the nonlinearity  $\hat{N}[\psi, \psi_x, |\psi|^2, (|\psi|^2)_x]$  satisfy the requirement of the  $\mathcal{PT}$  symmetry:  $V(-x) = V(x)$ ,  $W(-x) = -W(x)$ ,  $[\mathcal{PT}, \hat{N}] = 0$ .

### Acknowledgments

The work of Y.C. was supported by the NSFC under Grant Nos. 12001246 and 11947087, the NSF of Jiangsu Province of China (No. BK20190991) and the NSF of Jiangsu Higher Education Institutions of China (No. 19KJB110011). The work of Z.Y. was supported by the NSFC under Grant Nos. 11925108 and 11731014. The work of B.A.M. was supported, in part by the Israel Science Foundation though grant No. 1286/17.

## References

- [1] C. M. Bender and S. Boettcher. Real spectra in non-Hermitian Hamiltonians having PT symmetry. *Phys. Rev. Lett.*, 80(24):5243, 1998.
- [2] B. Bagchi and R. Roychoudhury. A new PT-symmetric complex Hamiltonian with a real spectrum. *J. Phys. A*, 33(1):L1, 2000.
- [3] B. Bagchi, C. Quesne, and M. Znojil. Generalized continuity equation and modified normalization in PT-symmetric quantum mechanics. *Mod. Phys. Lett. A*, 16(31):2047–2057, 2001.
- [4] Z. Ahmed. Real and complex discrete eigenvalues in an exactly solvable one-dimensional complex PT-invariant potential. *Phys. Lett. A*, 282(6):343–348, 2001.

- [5] B. Bagchi and C. Quesne. Pseudo-Hermiticity, weak pseudo-Hermiticity and  $\eta$ -orthogonality condition. *Phys. Lett. A*, 301(3-4):173–176, 2002.
- [6] B. Bagchi and C. Quesne. Non-Hermitian Hamiltonians with real and complex eigenvalues in a Lie-algebraic framework. *Phys. Lett. A*, 300(1):18–26, 2002.
- [7] Z. H. Musslimani, K. G. Makris, R. El-Ganainy, and D. N. Christodoulides. Optical solitons in PT periodic potentials. *Phys. Rev. Lett.*, 100(3):030402, 2008.
- [8] Z. Shi, X. Jiang, X. Zhu, and H. Li. Bright spatial solitons in defocusing Kerr media with PT-symmetric potentials. *Phys. Rev. A*, 84(5):053855, 2011.
- [9] S. Nixon, L. Ge, and J. Yang. Stability analysis for solitons in PT-symmetric optical lattices. *Phys. Rev. A*, 85(2):023822, 2012.
- [10] V. Achilleos, P. G. Kevrekidis, D. J. Frantzeskakis, and R. Carretero-González. Dark solitons and vortices in PT-symmetric nonlinear media: From spontaneous symmetry breaking to nonlinear PT phase transitions. *Phys. Rev. A*, 86(1):013808, 2012.
- [11] Z. Yan. Complex PT-symmetric nonlinear Schrödinger equation and Burgers equation. *Philos. T. R. Soc. A*, 371(1989):20120059, 2013.
- [12] Y. Lumer, Y. Plotnik, M. C. Rechtsman, and M. Segev. Nonlinearly induced PT transition in photonic systems. *Phys. Rev. Lett.*, 111(26):263901, 2013.
- [13] Z. Yan, Z. Wen, and C. Hang. Spatial solitons and stability in self-focusing and defocusing Kerr nonlinear media with generalized parity-time-symmetric Scarff-II potentials. *Phys. Rev. E*, 92(2):022913, 2015.
- [14] Z. Wen and Z. Yan. Dynamical behaviors of optical solitons in parity-time (PT) symmetric sextic anharmonic double-well potentials. *Phys. Lett. A*, 379(36):2025–2029, 2015.
- [15] Z. Yan, Z. Wen, and V. V. Konotop. Solitons in a nonlinear Schrödinger equation with PT-symmetric potentials and inhomogeneous nonlinearity: Stability and excitation of nonlinear modes. *Phys. Rev. A*, 92(2):023821, 2015.
- [16] A. Guo, G. J. Salamo, D. Duchesne, R. Morandotti, M. V. Ravat, V. Aimez, G. A. Siviloglou, and D. N. Christodoulides. Observation of PT-symmetry breaking in complex optical potentials. *Phys. Rev. Lett.*, 103(9):093902, 2009.
- [17] C. E. Rüter, K. G. Makris, R. El-Ganainy, D. N. Christodoulides, M. Segev, and D. Kip. Observation of parity-time symmetry in optics. *Nat. Phys.*, 6(3):192–195, 2010.
- [18] A. Regensburger, C. Bersch, M.-A. Miri, G. Onishchukov, D. N. Christodoulides, and U. Peschel. Parity-time synthetic photonic lattices. *Nature*, 488(7410):167–171, 2012.
- [19] G. Castaldi, S. Savoia, V. Galdi, A. Alù, and N. Engheta. PT metamaterials via complex-coordinate transformation optics. *Phys. Rev. Lett.*, 110(17):173901, 2013.
- [20] A. Regensburger, M.-A. Miri, C. Bersch, J. Näger, G. Onishchukov, D. N. Christodoulides, and U. Peschel. Observation of defect states in PT-symmetric optical lattices. *Phys. Rev. Lett.*, 110(22):223902, 2013.
- [21] B. Peng, S. K. Özdemir, F. Lei, F. Monifi, M. Gianfreda, G. L. Long, S. Fan, F. Nori, C. M. Bender, and L. Yang. Parity-time-symmetric whispering-gallery microcavities. *Nat. Phys.*, 10(5):394–398, 2014.
- [22] A. A. Zyablovsky, A. P. Vinogradov, A. A. Pukhov, A. V. Dorofeenko, and A. A. Lisyansky. PT-symmetry in optics. *Phys. Usp.*, 57(11):1063, 2014.
- [23] P.-Y. Chen and J. Jung. PT Symmetry and Singularity-Enhanced Sensing Based on Photoexcited Graphene Metasurfaces. *Phys. Rev. Appl.*, 5(6):064018, 2016.
- [24] K. Takata and M. Notomi. PT-Symmetric Coupled-Resonator Waveguide Based on Buried Heterostructure Nanocavities. *Phys. Rev. Appl.*, 7(5):054023, 2017.
- [25] H. Hodaei, A. U. Hassan, S. Wittek, H. Garcia-Gracia, R. El-Ganainy, D. N. Christodoulides, and M. Khajavikhan. Enhanced sensitivity at higher-order exceptional points. *Nature*, 548(7666):187, 2017.
- [26] B. Liu, H. Zhang, R. Zhong, X. Zhang, X. Qin, C. Huang, Y. Li, and B. A. Malomed. Symmetry breaking of quantum droplets in a dual-core trap. *Phys. Rev. A*, 99(5):053602, 2019.
- [27] E. A. Ultanir, G. I. Stegeman, and D. N. Christodoulides. Dissipative photonic lattice solitons. *Opt. Lett.*, 29(8):845–847, 2004.
- [28] K. G. Makris, R. El-Ganainy, D. N. Christodoulides, and Z. H. Musslimani. Beam dynamics in PT symmetric optical lattices. *Phys. Rev. Lett.*, 100(10):103904, 2008.
- [29] K. G. Makris, R. El-Ganainy, D. N. Christodoulides, and Z. H. Musslimani. PT-symmetric optical lattices. *Phys. Rev. A*, 81(6):063807, 2010.
- [30] K. G. Makris, R. El-Ganainy, D. N. Christodoulides, and Z. H. Musslimani. PT-symmetric periodic optical potentials. *Int. J. Theor. Phys.*, 50(4):1019–1041, 2011.
- [31] Z. H. Musslimani, K. G. Makris, R. El-Ganainy, and D. N. Christodoulides. Analytical solutions to a class of nonlinear Schrödinger equations with PT-like potentials. *J. Phys. A*, 41(24):244019, 2008.

- [32] C. Dai, X. Wang, and G. Zhou. Stable light-bullet solutions in the harmonic and parity-time-symmetric potentials. *Phys. Rev. A*, 89(1):013834, 2014.
- [33] S. Hu, X. Ma, D. Lu, Z. Yang, Y. Zheng, and W. Hu. Solitons supported by complex PT-symmetric Gaussian potentials. *Phys. Rev. A*, 84(4):043818, 2011.
- [34] J. Yang. Symmetry breaking of solitons in one-dimensional parity-time-symmetric optical potentials. *Opt. Lett.*, 39(19):5547–5550, 2014.
- [35] D. A. Zezyulin and V. V. Konotop. Nonlinear modes in the harmonic PT-symmetric potential. *Phys. Rev. A*, 85(4):043840, 2012.
- [36] B. Midya and R. Roychoudhury. Nonlinear localized modes in PT-symmetric Rosen-Morse potential wells. *Phys. Rev. A*, 87(4):045803, 2013.
- [37] H. Cartarius and G. Wunner. Model of a PT-symmetric Bose-Einstein condensate in a  $\delta$ -function double-well potential. *Phys. Rev. A*, 86(1):013612, 2012.
- [38] F. Single, H. Cartarius, G. Wunner, and J. Main. Coupling approach for the realization of a PT-symmetric potential for a Bose-Einstein condensate in a double well. *Phys. Rev. A*, 90(4):042123, 2014.
- [39] C. P. Jisha, L. Devassy, A. Alberucci, and V. C. Kuriakose. Influence of the imaginary component of the photonic potential on the properties of solitons in PT-symmetric systems. *Phys. Rev. A*, 90(4):043855, 2014.
- [40] F. Kh. Abdullaev, Y. V. Kartashov, V. V. Konotop, and D. A. Zezyulin. Solitons in PT-symmetric nonlinear lattices. *Phys. Rev. A*, 83(4):041805, 2011.
- [41] N. Moiseyev. Crossing rule for a PT-symmetric two-level time-periodic system. *Phys. Rev. A*, 83(5):052125, 2011.
- [42] C. P. Jisha, A. Alberucci, V. A. Brazhnyi, and G. Assanto. Nonlocal gap solitons in PT-symmetric periodic potentials with defocusing nonlinearity. *Phys. Rev. A*, 89(1):013812, 2014.
- [43] Sean Nixon, Lijuan Ge, and Jianke Yang. Stability analysis for solitons in PT-symmetric optical lattices. *Phys. Rev. A*, 85(2):023822, 2012.
- [44] H. Wang and D. N. Christodoulides. Two dimensional gap solitons in self-defocusing media with PT-symmetric superlattice. *Commun. Nonlinear Sci. Numer. Simul.*, 38:130–139, 2016.
- [45] S. V. Suchkov, A. A. Sukhorukov, J. Huang, S. V. Dmitriev, C. Lee, and Y. S. Kivshar. Nonlinear switching and solitons in PT-symmetric photonic systems. *Laser Photonics Rev.*, 10(2):177–213, 2016.
- [46] G. Burlak and B. A. Malomed. Stability boundary and collisions of two-dimensional solitons in PT-symmetric couplers with the cubic-quintic nonlinearity. *Phys. Rev. E*, 88(6):062904, 2013.
- [47] Yu. V. Bludov, V. V. Konotop, and B. A. Malomed. Stable dark solitons in PT-symmetric dual-core waveguides. *Phys. Rev. A*, 87(1):013816, 2013.
- [48] R. Fortanier, D. Dast, D. Haag, H. Cartarius, J. Main, G. Wunner, and R. Gutöhrlein. Dipolar Bose-Einstein condensates in a PT-symmetric double-well potential. *Phys. Rev. A*, 89(6):063608, 2014.
- [49] D. Dizdarevic, D. Dast, D. Haag, J. Main, H. Cartarius, and G. Wunner. Cusp bifurcation in the eigenvalue spectrum of PT-symmetric Bose-Einstein condensates. *Phys. Rev. A*, 91(3):033636, 2015.
- [50] C. Dai, X. Zhang, Y. Fan, and L. Chen. Localized modes of the  $(n+1)$ -dimensional Schrödinger equation with power-law nonlinearities in PT-symmetric potentials. *Commun. Nonlinear Sci. Numer. Simul.*, 43:239–250, 2017.
- [51] C. Dai, R. Chen, Y. Wang, and Y. Fan. Dynamics of light bullets in inhomogeneous cubic-quintic-septimal nonlinear media with PT-symmetric potentials. *Nonlinear Dynam.*, 87(3):1675–1683, 2017.
- [52] P. Li, D. Mihalache, and L. Li. Asymmetric solitons in parity-time-symmetric double-hump Scarf-II potentials. *Rom. J. Phys.*, 61:1028–1039, 2016.
- [53] R. J. Lombard and R. Mezhoud. The linear complex PT-symmetric potential. *Rom. J. Phys.*, 62:112, 2017.
- [54] P. Li and D. Mihalache. Symmetry breaking of solitons in PT-symmetric potentials with competing cubic-quintic nonlinearity. *Proc. Romanian Acad. A*, 19(1):61–68, 2018.
- [55] P. Li, L. Li, and D. Mihalache. Optical solitons in PT-symmetric potentials with competing cubic-quintic nonlinearity: existence, stability, and dynamics. *Rom. Rep. Phys.*, 70(1):408, 2018.
- [56] R. J. Lombard, R. Mezhoud, and R. Yekken. Complex potentials with real eigenvalues and the inverse problem. *Rom. J. Phys.*, 63:101, 2018.
- [57] J. Yang. Can parity-time-symmetric potentials support families of non-parity-time-symmetric solitons? *Stud. Appl. Math.*, 132(4):332–353, 2014.
- [58] Z. Yan, Y. Chen, and Z. Wen. On stable solitons and interactions of the generalized Gross-Pitaevskii equation with PT- and non-PT-symmetric potentials. *Chaos*, 26(8):083109, 2016.
- [59] Y. Chen, Z. Yan, and X. Li. One- and two-dimensional gap solitons and dynamics in the PT-symmetric lattice potential and spatially-periodic momentum modulation. *Commun. Nonlinear Sci. Numer. Simul.*, 55:287–297, 2018.



- [60] Y. Chen and Z. Yan. Solitonic dynamics and excitations of the nonlinear Schrödinger equation with third-order dispersion in non-Hermitian PT-symmetric potentials. *Sci. Rep.*, 6:23478, 2016.
- [61] Y. Chen, Z. Yan, D. Mihalache, and B. A. Malomed. Families of stable solitons and excitations in the PT-symmetric nonlinear Schrödinger equations with position-dependent effective masses. *Sci. Rep.*, 7(1):1257, 2017.
- [62] Y. Chen and Z. Yan. Stable parity-time-symmetric nonlinear modes and excitations in a derivative nonlinear Schrödinger equation. *Phys. Rev. E*, 95(1):012205, 2017.
- [63] Z. Wen and Z. Yan. Solitons and their stability in the nonlocal nonlinear Schrödinger equation with PT-symmetric potentials. *Chaos*, 27(5):053105, 2017.
- [64] Z. Yan and Y. Chen. The nonlinear Schrödinger equation with generalized nonlinearities and PT-symmetric potentials: Stable solitons, interactions, and excitations. *Chaos*, 27(7):073114, 2017.
- [65] Y. Shen, Z. Wen, Y. Yan, and C. Hang. Effect of PT symmetry on nonlinear waves for three-wave interaction models in the quadratic nonlinear media. *Chaos*, 28(4):043104, 2018.
- [66] Y. Chen, Z. Yan, and W. Liu. Impact of near-PT symmetry on exciting solitons and interactions based on a complex Ginzburg-Landau model. *Optics Express*, 26(25):33022–33034, 2018.
- [67] Y. Chen, Z. Yan, and D. Mihalache. Stable flat-top solitons and peakons in the PT-symmetric  $\delta$ -signum potentials and nonlinear media. *Chaos*, 29(8):083108, 2019.
- [68] T. Mayteevarunyoo, B. A. Malomed, and A. Roeksabutr. A solvable model for solitons pinned to a PT-symmetric dipole. *Phys. Rev. E*, 88(2):022919, 2013.
- [69] L. Wang, B. A. Malomed, and Z. Yan. Attraction centers and parity-time-symmetric delta-functional dipoles in critical and supercritical self-focusing media. *Phys. Rev. E*, 99(5):052206, 2019.
- [70] Y. V. Kartashov, V. V. Konotop, and L. Torner. Topological states in partially-PT-symmetric azimuthal potentials. *Phys. Rev. Lett.*, 115(19):193902, 2015.
- [71] Y. V. Kartashov, C. Hang, G. Huang, and L. Torner. Three-dimensional topological solitons in PT-symmetric optical lattices. *Optica*, 3(10):1048–1055, 2016.
- [72] B. A. Malomed. Vortex solitons: Old results and new perspectives. *Physica D*, 399:108–137, 2019.
- [73] V. V. Konotop, J. Yang, and D. A. Zezyulin. Nonlinear waves in PT-symmetric systems. *Rev. Mod. Phys.*, 88(3):035002, 2016.
- [74] Y. He, B. A. Malomed, and D. Mihalache. Localized modes in dissipative lattice media: an overview. *Philos. T. R. Soc. A*, 372(2027):20140017, 2014.
- [75] D. Mihalache. Multidimensional localized structures in optical and matter-wave media: A topical survey of recent literature. *Rom. Rep. Phys.*, 69(1):403, 2017.
- [76] R. El-Ganainy, K. G. Makris, M. Khajavikhan, Z. H. Musslimani, S. Rotter, and D. N. Christodoulides. Non-Hermitian physics and PT symmetry. *Nat. Phys.*, 14(1):11–19, 2018.
- [77] D. N. Christodoulides and J. Yang. *Parity-time Symmetry and its Applications*, volume 280. Springer, 2018.
- [78] B. A. Malomed and D. Mihalache. Nonlinear waves in optical and matter-wave media: A topical survey of recent theoretical and experimental results. *Rom. J. Phys.*, 64:106, 2019.
- [79] D. Mihalache. Localized structures in optical and matter-wave media: a selection of recent studies. *Rom. Rep. Phys.*, 73:403, 2021.
- [80] T. Cazenave. *Semilinear Schrödinger Equations*, volume 10. American Mathematical Soc., 2003.
- [81] M. J. Ablowitz and Z. H. Musslimani. Spectral renormalization method for computing self-localized solutions to nonlinear systems. *Opt. Lett.*, 30(16):2140–2142, 2005.
- [82] J. Yang and T. I. Lakoba. Universally-convergent squared-operator iteration methods for solitary waves in general nonlinear wave equations. *Stud. Appl. Math.*, 118(2):153–197, 2007.
- [83] J. Yang. Newton-conjugate-gradient methods for solitary wave computations. *J. Comput. Phys.*, 228(18):7007–7024, 2009.
- [84] J. Yang. *Nonlinear waves in integrable and nonintegrable systems*. SIAM, 2010.
- [85] L. E. Gendenshtein. Derivation of exact spectra of the Schrödinger equation by means of supersymmetry. *Jetp Lett*, 38(6):356–359, 1983.
- [86] Y. Chen, Z. Yan, and D. Mihalache. Soliton formation and stability under the interplay between parity-time-symmetric generalized Scarf-II potentials and Kerr nonlinearity. *Phys. Rev. E*, 102(1):012216, 2020.
- [87] H. Cartarius, D. Haag, D. Dast, and G. Wunner. Nonlinear Schrödinger equation for a-symmetric delta-function double well. *Journal of Physics A*, 45(44):444008, 2012.
- [88] A. S. Rodrigues, K. Li, V. Achilleos, P. G. Kevrekidis, D. J. Frantzeskakis, and C. M. Bender. PT-symmetric double well potentials revisited: bifurcations, stability and dynamics. *Rom. Rep. Phys.*, 65:5–26, 2013.

- [89] H. Susanto, R. Kusdiantara, N. Li, O. B. Kirikchi, D. Adzkiya, E. R. M. Putri, and T. Asfihani. Snakes and ghosts in a parity-time-symmetric chain of dimers. *Phys. Rev. E*, 97(6):062204, 2018.
- [90] B. A. Malomed. Multidimensional solitons: Well-established results and novel findings. *The European Physical Journal Special Topics*, 225(13):2507–2532, 2016.
- [91] Y. V. Kartashov, G. E. Astrakharchik, B. A. Malomed, and L. Torner. Frontiers in multidimensional self-trapping of nonlinear fields and matter. *Nat. Rev. Phys.*, 1(3):185–197, 2019.
- [92] D. Dast, D. Haag, H. Cartarius, J. Main, and G. Wunner. Eigenvalue structure of a Bose–Einstein condensate in a PT-symmetric double well. *J. Phys. A*, 46(37):375301, 2013.